Interaction of gold cationic nanoparticles with blood
cells and their distribution in the model organism

BAKALÁŘSKÁ PRÁCE

Studijní program:

SPECIALIZACE VE ZDRAVOTNICTVÍ

Autor: Michal Šrámek

Vedoucí práce: MUDr. Zdeněk Hodný, CSc.

České Budějovice 2019

Prohlášení

Prohlašuji, že svoji bakalářskou práci s názvem *Interaction of gold cationic nanoparticles with blood cells and their distribution in the model organism* jsem vypracoval samostatně pouze s použitím pramenů v seznamu citované literatury.

Prohlašuji, že v souladu s § 47b zákona č. 111/1998 Sb. v platném znění souhlasím se zveřejněním své bakalářské práce, a to v nezkrácené podobě elektronickou cestou ve veřejně přístupné části databáze STAG provozované Jihočeskou univerzitou v Českých Budějovicích na jejích internetových stránkách, a to se zachováním mého autorského práva k odevzdanému textu této kvalifikační práce. Souhlasím dále s tím, aby touž elektronickou cestou byly v souladu s uvedeným ustanovením zákona č. 111/1998 Sb. zveřejněny posudky školitele a oponentů práce i záznam o průběhu a výsledku obhajoby bakalářské práce. Rovněž souhlasím s porovnáním textu mé bakalářské práce s databází kvalifikačních prací Theses.cz provozovanou Národním registrem vysokoškolských kvalifikačních prací a systémem na odhalování plagiátů.

V Českých Budějovicích dne 03.05.2019 …………………………

podpis

Interakce zlatých kationických nanočástic s krevními buňkami a jejich distribuce v modelovém organismu

Abstrakt

Kationické zlaté nanočástice (GNPs) jsou vhodnými kandidáty pro doručování léčiv, zobrazování v biomedicíně a pro cílenou léčbu nádorových onemocnění. Vzhledem k jejich unikátním fyzikálně-chemickým vlastnostem mohou být využity především pro tzv. cílenou fototermální léčbu nádorů. Během buněčné internalizace hraje klíčovou roli především velikost, tvar a povrchový náboj nanočástice. Různé typy nanočástic vstupují do buňky různými cestami. Je známo, že kationické zlaté nanotyčinky (GNRs) jsou normálními i nádorovými buňkami snadno vychytávány, přičemž jsou během endocytózy hromaděny uvnitř vezikulárních struktur.

Před zahájením aplikace GNRs v biomedicíně pro různé typy účelů (jako je fototermální terapie, cílené nosiče léčiv, fluorescenční sondy, těhotenský test atd.) je nutné nejdříve určit jejich biologickou bezpečnost a reakci organismu obecně. V naší laboratoři se zaměřujeme především na aplikace GNRs ve fototermální terapii. Jejím principem je nahromadění kationických GNRs v nádorové tkáni, kde po ozáření světelným paprskem o frekvenci blízké infračervenému (NIR) světlu transformují světlo na teplo, čímž termálně poškodí buňky.

Během této studie bylo ukázáno pomocí mikroskopického vyšetření krve, že po její inkubaci s kationickými GNRs *in vitro* dochází k interakci GNRs s bílými krvinkami a trombocyty. Dále bylo ukázáno pomocí histologie a fluorescenční mikroskopie, že po aplikaci *in vivo* se kationické GNRs v největší míře akumulují v myší slezině. Získaná data přispěla k porozumění distribuce a toxicity kationických GNRs na úrovni buňky a organismu a byla publikována v rámci komplexní studie v časopise Biomaterials.

Klíčová slova
Zlaté nanočástice; nádorové onemocnění; fototermální terapie; krev; tkáně

Interaction of gold cationic nanoparticles with blood cells and their distribution in the model organism

Abstract

Cationic gold nanoparticles (GNPs) are attractive candidates for drug delivery, biomedical imaging and targeted anti-cancer therapy. Due to their unique physical-chemical properties, they have great potential, especially for so-called targeted photothermal cancer therapy. Nanoparticle properties such as size, shape and surface charge play a key role in the internalization process and different types of NPs can enter cells by various pathways. It has been reported, that specific cationic gold nanorods (GNRs) preparations are taken up by both normal and cancer cells in large amounts. The nanoparticles were shown to accumulate inside vesicular structures.

Prior to the start with an application of cationic GNRs in biomedicine for different kind of purposes (such as photothermal therapy, targeted drug/gene delivery carriers, fluorescence probes, pregnancy test etc.), it is necessary at first to determine their biological safety and organism's response in general. In our laboratory, we are focused mainly on the application of GNRs in photothermal therapy. That consists of cationic GNRs accumulated in tumour tissue, where they transform light into heat upon irradiation by near-infrared (NIR) light, thereby thermally damaging nearby cells.

During the study, it was shown by microscopic examination of the blood that after incubation of blood with cationic GNRs in vitro, the interaction of GNRs with white blood cells and platelets was observed. Further, using histology and fluorescence microscopy it was shown that after in vivo application the cationic GNRs are mostly accumulated in mouse spleen. The obtained data contributed to an understanding of cationic GNRs distribution and toxicity at the level of the cell and organism and were published as a part of the complex study in Biomaterials journal.

Keywords

Table of Contents

1. Introduction to Nanoparticles

The chemical design and synthesis of nanoparticles have fuelled the growth of nanotechnology and their biomedical applications. Colloidal gold nanoparticles (GNPs) are a promising drug delivery platform for targeted cancer therapies (Hirsch *et al.* 2003). In recent years, several clinical trials of nanoparticle-based anticancer therapeutics involving colloidal gold with unique optical properties have been conducted (Dobrovolskaia *et al.* 2009).

1.1 Properties of Gold Nanoparticles

Distinct and tunable optical, electronic, or magnetic properties of nanometre-sized objects founded quickly developing the field of nanotechnology research (Chithrani *et al.* 2006). The word nano, derived from the Greek *nanos*, meaning dwarf, is used to describe any material or property which occurs with dimensions on the nanometre scale (1 – 100 nm), which can exhibit in vivid colours (Dreaden *et al.* 2012).

Gold is the quintessential noble element, highly unreactive by nature. The GNPs have a high surface area that has a localized surface plasmon resonance (LSPR) effect. The intense colour of nanoparticles arises from the collective excitation of their conduction electrons excited by a light beam of significantly greater wavelength than the particle size, or LSPR modes, which results in photon absorption at wavelengths which varies mostly with nanoparticle aspect ratio (Fig. 1), shell thickness (Fig. 2) or for example galvanic displacement by gold (Fig. 3). This excitation is very powerful and allows the visualization of single nanoparticles (Raschke *et al.* 2003). For GNPs, the visible light meets the condition for excitation (approx. 400 – 700 nm) and near-infrared light (close-infrared light: 650 – 900 nm, *i.e.*, NIR light: 800 – 2500 nm). Therefore, the GNPs solution appears with colour (Jain *et al.* 2006). The presence of other particles and their relative spacing also influence the frequency of LSPR, while the aggregation of the particles changes the colour of the solution (Su *et al.* 2003).

One of the most important aspects is a controllable synthesis because the shape and size (or aspect ratio in case of nanorods) of nanoparticles is controlled by synthesis processes. Preparation of gold rod-shaped nanoparticles – gold nanorods (GNRs) is demonstrated by high-yield synthesis in cetyltrimethylammonium bromide (CTAB) via seed-mediated growth (Fig. 1). This method produces a solution of the colloidal nanorods (for details, see Section 3.3.1).
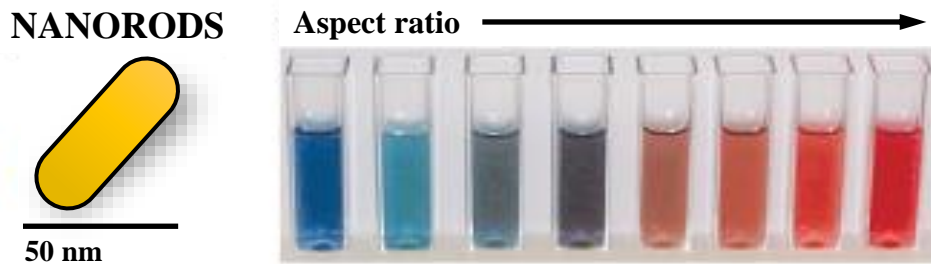
NANORODS

Aspect ratio ➝

50 nm

Fig. 1 – The aspect ratio related to the colour of the gold nanorods
(Dreaden *et al.* 2012).

In another typical synthesis of GNPs, silica nanoparticle cores are synthesized by the base-catalysed condensation of orthosilicate (Stöber *et al.* 1968). Nanoparticles are synthesized from the aqueous reduction of chloroauric acid by tetrakis(hydroxymethyl) phosphonium chloride (THPC) and adsorbed onto silica cores where subsequently form a conformal nanoshell (Fig. 2).

NANOSHELLS

⬅ **Shell thickness**

140 nm

Fig. 2 – The shell thickness related to the colour of the silica-gold nanoshells
(Dreaden *et al.* 2012).

Another example is the synthesis of so-called nanocages. Gold nanocages (Fig. 3) or frames are produced by reacting Au(III) with silver nanocubes produced from the polyol reduction of silver nitrate which further reacts to form porous Au nanocages (Lu *et al.* 2007).

NANOCAGES

% gold ➝

50 nm

Fig. 3 – The percentage of gold in nanocage solution related to colour
(Dreaden *et al.* 2012).

Regarding the synthesis of nanoparticles in general, there exist several types of materials and many synthetic approaches, how to create nanoparticles with a lot of different shapes (see Fig. 17 in attachments). Specifically, triangular or for example prismatic

9

nanoparticles have been obtained by photoreduction, seed-mediated growth, plasmon–driven synthesis and biosynthesis as well.

The LSPR mentioned above is closely connected to an absorption maximum of gold nanoparticles. Because gold nanospheres have only one dimension, they have only one absorption maximum (around 520 nm). In contrast, for GNRs the group of El-Sayed shown to have two types of LSPR (Eustis and El-Sayed 2006), first one due to the transverse oscillation of the electrons around 520 nm for gold and the second one due to the longitudinal LSPR at longer wavelengths for various aspect ratios.
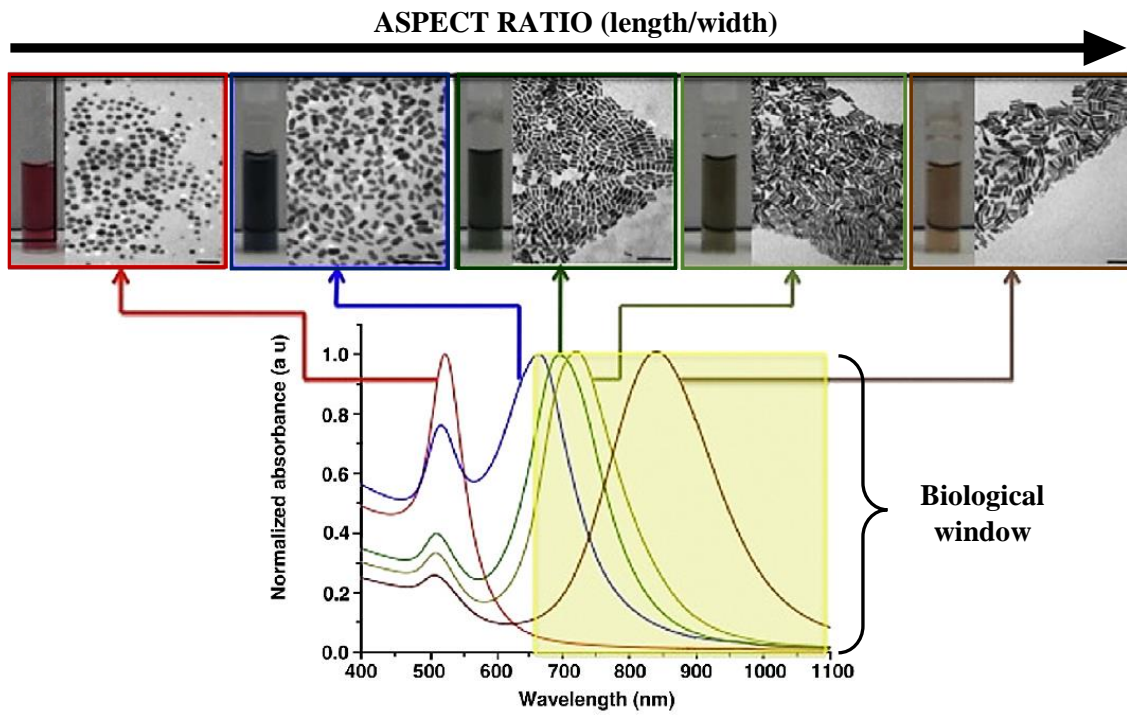
Fig. 4 – UV–Vis spectra, TEM and photographs of aqueous solutions of GNRs with a different aspect ratio (Alkilany *et al.* 2012). Scale bar 100 nm.

The transverse LSPR is not dependent on the aspect ratio and it is at the same wavelength as the LSPR of spheres (Fig. 4). The longitudinal LSPR is increased if the aspect ratio is higher.

For optical bioimaging of GNPs or GNRs, the LSPR plays a central role, but it is also important in which part of the electromagnetic spectrum is located. In the Fig. 4 the yellow region called biological window or also known as a near-infrared (NIR) window is shown. NIR light is within the range 700 – 2500 nm and, importantly for biomedical applications, can penetrate biological tissues such as skin and blood more efficiently than visible light because these tissues scatter and absorb less light at longer wavelengths (Smith *et al.* 2009). This region is basically divided into two biological windows – the

first spans wavelengths 650 nm to 950 nm and the second starts at wavelengths 1000 to 1200 nm. Unfortunately, the effect of NIR penetration diminishes owing to increased absorption by water and lipids at wavelengths longer than 950 nm, so for optical imaging of live animals, the first biological window at wavelengths between 650 nm and 950 nm is mostly used.

1.2   *Functionalization of Gold Nanoparticles*

Surface modification of nanoparticles brings the advantages of increasing stability, facilitating surface chemistry, tuning physicochemical properties and broadening practical applications. Colloidal GNPs are usually surrounded by stabilizing molecules, which one of their ends is either adsorbed or chemically linked to the gold surface, while the other endpoints towards the solution and provides colloidal stability (Sperling *et al.* 2008). After synthesis of the particles, other stabilizer molecules in a ligand exchange reaction can replace the stabilizer molecules. As thiol moieties bind with high affinity to gold surfaces, thiol-modified ligands are used most frequently (Templeton *et al.* 2000). Ligand exchange is motivated by various reasons, mainly to adjust the surface properties of the particles by choosing the specific surfactant molecules.

Another important rationale to modify the surface of nanoparticles is, for instance, to increase the stability and solubility of nanoparticles, or to avoid the degradation of the nanoparticle surface in the blood by enzymes.
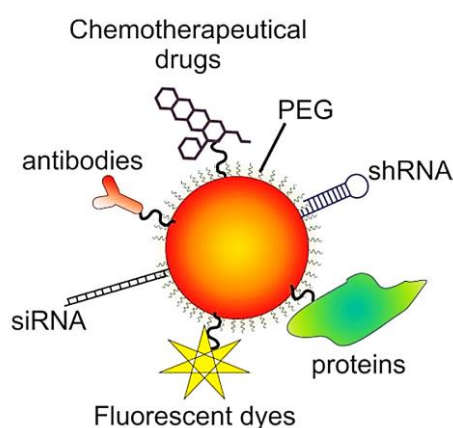

Fig. 5 – Optional functionalization of GNRs
(Roma-Rodrigues *et al.* 2017).

The binding of a hydrophilic polymer on the surface of GNPs increases hydration of the particle ensures a better solubility and their protection against surrounding environment, for example, reduces opsonisation and absorption by macrophages *in vivo* (Moghimi and Szebeni 2003).

Application of GNPs for therapeutic or diagnostic purposes involves functionalization of nanomaterials with specific biomolecules such as peptides, ligands or different chemical groups to improve their biocompatibility and to achieve specific different purposes. For therapeutic purposes, after functionalization with polyethylene glycol (PEG) for higher biocompatibility, colloidal GNPs may be in next step immobilized with a variety of molecules (Fig. 5), including chemotherapeutic drugs, antibodies, small interference RNAs (siRNA), short hairpin RNAs (shRNA), fluorescent dyes, proteins, or a combination of several biomolecules for targeting of the specific cells or disease sites (Roma-Rodrigues *et al.* 2017).

1.3 Applications of Gold Nanoparticles in Biomedicine

As mentioned above, GNPs have shown exceptional optical properties suitable for a wide range of applications and their application in clinical practice depends not only on their size but also on solubility and charge (McNeil 2005). Actually, two research groups initiated plasmonic photothermal therapy for cancer – Lin and co-workers (Pitsillides *et al.* 2003) photolyzed lymphocytes using spherical gold nanoparticles in combination with a pulsed visible laser. Halas and co-workers (Hirsch *et al.* 2003) photodestructed breast carcinoma cells and tumours in mice using silica/gold core/shell nanoparticles. Under NIR laser irradiation could be released drugs or genes from GNPs (Huang *et al.* 2009) for photothermal therapy, lithography or just imaging (Alkilany *et al.* 2012)
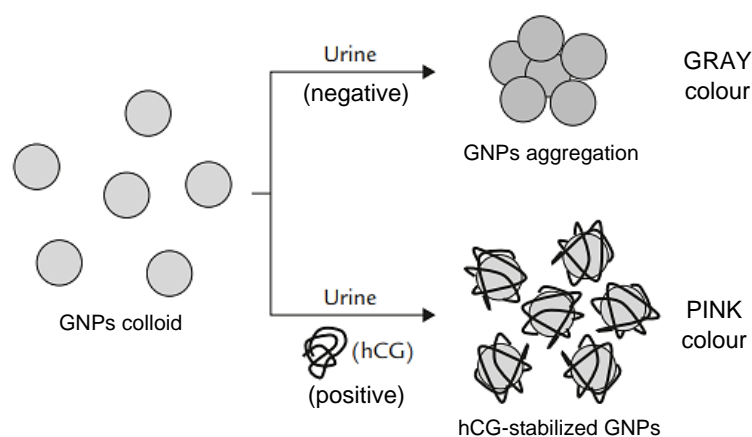
Fig. 6 – Diagram shows the reaction between human gonadotropin (hCG) and GNPs utilized in pregnancy test (Rojanathanes *et al.* 2008).

Intense photophysical properties of GNPs allow also their use in biodiagnostic assays (Dreaden *et al.* 2012). Basic biodiagnostic immunochromatography technique used by various hospital facilities is a pregnancy test (Fig. 6). Generally, the urine pregnancy tests measure human chorionic gonadotropin (hCG), which is secreted by the trophoblastic

cells of the placenta soon after implantation of the fertilized egg into the uterine wall (Chard 1992). This test is based on the significant difference in colour change due to the aggregation of the particles. Binding of hCG on the surface of GNPs makes pregnancy-positive mixture pink, while the pregnancy-negative mixture, where hCG is not present and GNPs aggregate, turns grey.

Because of their facile surface chemistry, GNPs can be conjugated with antibodies and thus broaden their application. Development of immunochemistry-based applications of the GNPs for biological studies was published by Faulk and Taylor (Faulk and Taylor 1971) who described a method of antibody conjugation with colloidal gold for direct electron microscopy visualization of the surface antigens of *Salmonellae*. Furthermore, GNPs-antibody conjugates allow real-time detection of the penetration of gold into living cells at the level of a single particle and even for the estimation of their amount (Klein *et al.* 2010). Another feature of GNPs is to absorb copious amounts of X-ray radiation and it can be utilised to enhance cancer radiation therapy or increase imaging contrast in diagnostic computed tomography (CT) scans (Dreaden *et al.* 2012).

1.4   *Recent in vivo Studies of Gold Nanoparticles*

For potential biomedical applications, quantitative and qualitative studies of the cellular uptake of GNPs with respect to their size and shape are required. This is also important for assessing nanoparticle toxicity, for development and improvement of GNPs imaging, drug delivery, designing multifunctional nanoparticles and therapeutic applications in general. Both safety and drug-delivery performance depend on the disposal and clearance of the colloids. The disposal and clearance also depend on a variety of characteristics of the nanoparticles, including their size (Chapter 1.1) and surface charge (Chapter 1.3).

1.4.1   *Blood*

When the GNPs are applied *in vivo* intravenously, the blood elements and blood cells will interact with them practically immediately. Blood elements can bind to GNPs (described in Section 1.4.2) and blood cells can play the main role in the further distribution of these particles into the organs.

The composition of blood can be examined after separation into three parts while centrifuged - the top part consists of clear plasma, which forms about 55% of blood total volume, the middle part is white layer which forms about 45% of total blood volume and it contains white blood cells (WBCs), such as granulocytes (neutrophils, eosinophils and
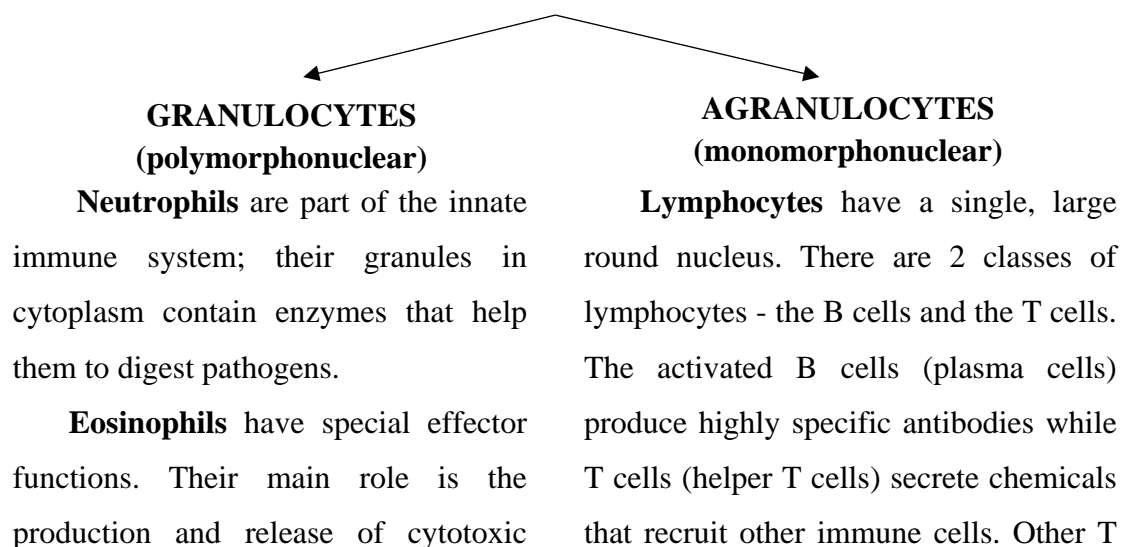
basophils), agranulocytes (lymphocytes and monocytes) and platelets, and the bottom part is full of the red blood cells (RBCs). Plasma contains mainly water (91%), but also important substances (Dean 2005), such as 7% of proteins (albumin, clotting factors, antibodies, enzymes), 2% of nutrients (amino acids, glucose or lipids), hormones (erythropoietin, insulin) and electrolytes (sodium, potassium, calcium). It is known, that all plasma components could play a role in the cellular uptake of GNPs (Chithrani *et al.* 2006), as specified in detail in Section 1.4.2.

1.4.1.1 Red Blood Cells

The bone marrow is responsible for the production and release of RBCs into the circulation. RBCs have a diameter of approximately 7 μm. Circulation of each RBC in the body lasts around 120 days. Damaged or old RBCs are removed by macrophages localized in the spleen and liver. Number of human RBCs is from 4.3×10^6 to 5.7×10^6 per μl (for male) or from 3.8×10^6 to 4.9×10^6 per 1 μl (for female). All mammals have matured RBCs without a nucleus. Thus RBCs have space and ability to store haemoglobin for transportation of oxygen (O_2) and carbon dioxide (CO_2) and thanks to their biconcave shape, they have increased surface area for better diffusion of both gases (Maton and Prentice-Hall 1993).

1.4.1.2 White Blood Cells

All WBCs are part of the immune system. Their role is to protect the body against both infectious disease and foreign invaders. WBCs appear in many different shapes and sizes. Some cells have nuclei with multiple lobes and contain pockets of granules in their cytoplasm (granulocytes). Another WBCs contains one large, round nucleus (Dean 2005).

GRANULOCYTES
(polymorphonuclear)

Neutrophils are part of the innate immune system; their granules in cytoplasm contain enzymes that help them to digest pathogens.

Eosinophils have special effector functions. Their main role is the production and release of cytotoxic

AGRANULOCYTES
(monomorphonuclear)

Lymphocytes have a single, large round nucleus. There are 2 classes of lymphocytes - the B cells and the T cells. The activated B cells (plasma cells) produce highly specific antibodies while T cells (helper T cells) secrete chemicals that recruit other immune cells. Other T

substances from granules (reactive oxygen species) and also lymphokines (TGFß, IL-2, IL-6, TNFα).

Basophils appear in inflammatory reactions (allergies). Allergy reaction is manifested mainly via the vasodilator histamine. They also contain the anticoagulant heparin, which prevents blood from clotting too quickly.

cells (cytotoxic) attack virally infected cells**.**

Monocytes are young WBCs that develop into macrophages in tissues. There they provide an immediate defence because they can phagocytose and digest pathogens. Macrophages also present the foreign proteins (antigens) to other immune cells, triggering an immune response (Hořejší and Bartůňková 2005).

1.4.1.3 Platelets

The origin of platelet comes from megakaryocytes which release from their membrane irregularly shaped platelets into the bloodstream (Maton and Prentice-Hall 1993). The function of platelets is to form a blood clot after their activation to protect against bleeding. Platelets number range is 1.5 x 10^5 to 4.5 x 10^5 per µl. Thus, there is about 1 platelet for every 10 RBCs (see Section 1.4.1.1). They circulate for about 9 days in the blood and ends their lifespan in the spleen (Dean 2005)

1.4.2 Protein Corona

Like many nanoparticles, gold colloids injected into the bloodstream are quickly coated by plasma proteins (Zanganeh *et al.* 2016), what is known professionally as protein corona. Some of the absorbed proteins remain associated with the particles for a significant portion of its therapeutic lifetime, and the properties of the protein coat may ultimately define the biological response to the nanoparticles, including influence on cellular uptake, organ accumulation, and route of clearance (Dobrovolskaia *et al.* 2009). There has been shown that colloidal gold particles adsorb plasma proteins (detail composition of plasma in Section 1.4.1) and it influences clearance by immune cells (different cell types, Section 1.4.1.2) (Chithrani *et al.* 2006), but neither the size of the protein-bound colloid particles nor the individual molecular identities of the bound proteins have been examined.

Among 7% of all plasma proteins (mentioned in Section 1.4.1), the albumin and globulins of all four types have the major representation (Fig. 7).

In the study of Zarska *et al.* is described that human serum albumin (HSA) provide stability and affects *in vivo* properties of GNRs (Zarska *et al.* 2016). The stability process

is described as the binding between HSA and the GNRs, a similar principle to the pregnancy test (Fig. 6). In the Payne lab, they have observed that albumin is the most abundant protein adsorbed on polystyrene GNPs, semiconductor quantum dots, and colloidal gold GNPs following exposure to serum proteins (Fleischer and Payne 2014). Albumin is also a component of serum used in media for *in vitro* cell cultures – for example, bovine serum albumin (BSA) in Dulbecco's Modified Eagle Medium (DMEM).
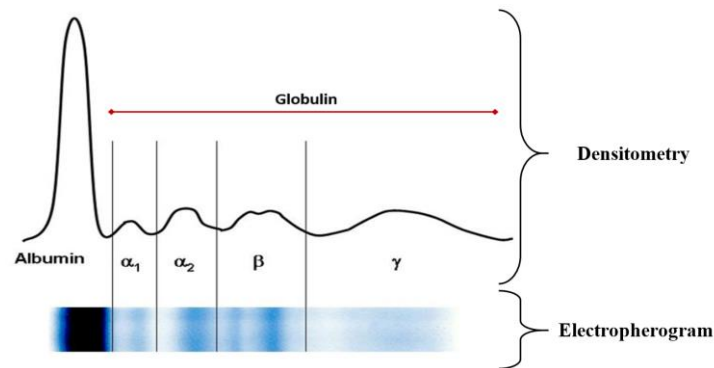

Fig. 7 – The representation of plasma proteins.
(Reposted from MUDr. Lenka Fialová, CSc., 2008).

Binding of proteins to nanoscale gold colloid is mediated due to electrostatic effects. Sequential model of protein binding describes that the cationic proteins initially bind the colloid (essentially coating the negative charges) followed by binding of anionic proteins to the cationic protein coat (Salvadormorales *et al.*, 2006). Dynamic light scattering (DLS) is used to determine the size distribution profile of colloids in suspension with polymers. DLS measures a particle's hydrodynamic diameter. As mentioned by Dobrovolskaia *et al.*, the diameter is increased in the case of the hydrodynamic size of citrate-stabilized gold colloids after the incubation of particles with plasma (Dobrovolskaia *et al.* 2009). This increase in particle diameter and a decrease in absolute zeta potential[1] are consistent with adsorption of positively or neutrally charged proteins to the surface of the colloidal particles.

---

[1] Zeta potential is the electrical charge that is generated on the interface of particles surface and the aqueous solution. The measurement technique is based on the indirect measurement obtained during the electro-kinetic experiments (Honary a Zahir 2013).

1.4.3 Exposure of Gold Nanoparticles in Rodents

Most published studies focus on measuring the biodistribution of GNPs in animal models (for example Niidome *et al.* (2006), Akiyama *et al.* (2009), Aillon *et al.* (2009), Balasubramanian *et al.* (2010) and also our study Zarska *et al.* (2018)). The general approach of these studies involves in most cases injecting or otherwise introducing a solution of GNPs into an animal at a selected dose, waiting for a specified amount of time, sacrificing the animal and elemental analysis of various organs to quantify the gold content in the organs.

All the studies follow basic diagram starting from the fabrication of desired particles (Fig. 8-A) and the characterization of their size, shape, structure, charge by transmission (TEM) or scanning electron microscopy (SEM), DLS or for example ultraviolet-visible (UV-VIS) spectroscopy. In the second step (Fig. 8-B) experiments focus on the functionalization of the particle surface with appropriate ligands (as mentioned in Chapter 1.2), including poly(ethylene glycol) methyl ether thiol (PEG-SH) or poly(ethylene oxide) (PEO) molecules, as well as opsonisation with blood plasma proteins. Administration of GNPs (Fig. 8-C) is made by using selected doses and routes of exposure, including intravenous, intraperitoneal, respiratory, or even gastrointestinal.
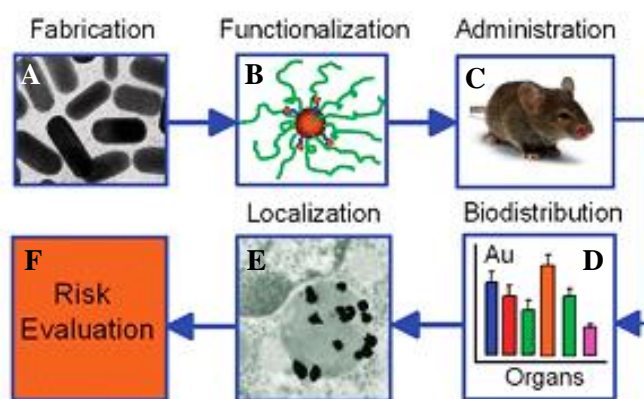

Fig. 8 – Scheme of biodistribution and nanotoxicology
experiments (Khlebtsov and Dykman 2011).

The biodistribution of GNPs into organs (Fig. 8-D) is generally determined according to a selected time-dependent scheme of tissue sampling. Samples can be analysed by radioactive analysis, instrumental neutron activation analysis, atomic absorption spectroscopy (AAS) or more sensitively by 'inductively coupled plasma mass spectrometry' (ICP-MS). Structures related to localisation of GNPs (Fig. 8-E) can be identified histologically and, at the cellular levels, by confocal microscopy or SEM/TEM.

The final step is the integration of data (Fig. 8-F) for the biological characterization of GNRs effects as Khlebtsov and Dykman showed (Khlebtsov and Dykman 2011), the evaluation of possible risks both at cellular (localisation, perturbation, cytotoxicity, genotoxicity, apoptosis/necrosis, etc.) and organism levels (organ distribution, accumulation and clearance/excretion, degradation and metabolism, immunogenicity, and inflammation). Before clarifying any specific experiments, for the basic outline, are below listed already published recent studies (in the last about 15 years) regarding the topics such as *in vivo* biodistribution and cytotoxicity. All studies are summarized in Tab. 3 in the attachments.

At first, in 2004 Hainfeld *et al.* used commercial GNPs (Hainfeld *et al.* 2004) with dimensions 1.9 nm, obtained from Nanoprobes, Inc. (Yaphank, New York) to improve X-ray therapy of tumours. After the two-week exposition of GNPs in mice, the organs were examined. The majority of nanoparticles was accumulated in the kidney followed by tumour mass. The tumour uptake was 1.8 times higher than the uptake of liver per g tissue. Hainfeld *et al.* repeated his work two years later (Hainfeld *et al.* 2006) with the same GNPs as a contrast agent for X-ray imaging, but with higher doses and longer duration. Colloidal GNPs were injected intravenously into mice and their biodistribution was measured by atomic absorption spectroscopy. Retention in liver and spleen was low with the elimination of nanoparticles by the kidneys.

Another study clearly shows a marked decrease in 33 nm colloidal GNPs uptake by the liver and spleen compared to a vector that targets GNPs to a tumour only. The vector consists of thiol-derivatized PEG and recombinant human tumour necrosis factor (TNF) that are directly bound onto the surface of the GNPs (Paciotti *et al.* 2004). Over time, the accumulation of nanoparticles was apparent in the skin and tissues surrounding the tumour. Paciotti *et al.* used the physical state of the particles for their tracking in the completely stabilized monodispersed state appeared red-burgundy in colour, while in a precipitated state the particles appeared black. Bergen *et al.* show that the biodistribution of nanoparticles is dependent on a complex set of variables (cell type, particle size and charge of bounded polymer) after using 50, 80, 100, 150 and 200 nm gold colloids (Bergen *et al.* 2006). A nanoparticle platform based on gold colloids unmodified or modified with thiolated polymers (PEG_{5000}-SH or galactose-PEG_{5000}-o-pyridyldisulfide) was used in their study to identify hepatocyte uptake.

Very interesting approach performed in 2006 by Niidome *et al* is 'PEG-modified gold nanorods for *in vivo* applications' (Niidome *et al* 2006). Authors injected colloidal

GNRs (0.5-0.9 mM) into the mice via the tail vein. Mice were sacrificed 0.5, 3, 6, 12, 24, and 72 hours later and gold content in blood and organs was quantified by ICP–MS. The amount of gold in the blood decreased in a time-dependent manner when no gold was observed after 72 hours. In the liver, 35% of the injected dose was accumulated at 72 hours. Only a small amount of gold was found in other organs. Study of Balogh *et al.* (2007) showed for the first time that the size of GNPs can greatly affect biodistribution into organs and tumour (Balogh *et al.* 2007). They used 5, 11, 22 nm gold composite nanodevices with a positive, negative or neutral charge. An important finding of this study is that not only the size but also the charge can influence the organ/tissue targeting or cause excretion of the nanodevices.

Saudaskas *et al.* demonstrated that intravenously injected GNPs (2 and 40 nm) were accumulated primarily in the liver Kupffer cells (Sadauskas *et al.* 2007). However, intraperitoneally injected GNPs showed a delayed uptake in the liver and a moderate uptake in mesenteric lymph nodes, spleen and small intestine. This data indicates the way of an injection of GNPs influences their organ distribution and should be considered before application. In the following study, they revealed the fate of 40 nm GNPs after intravenous injections (Sadauskas *et al.* 2009). Colloidal GNPs were identified in almost all Kupffer cells one day after the injection, but the fraction of gold-loaded cells gradually decreased to about one fifth after 6 months. That reports that inert GNPs injected intravenously are being removed from the circulation primarily by Kupffer cells of the liver.

Different experiments with an exposition of 10, 50, 100 and 250 nm GNPs described by De Jong *et al.* show the distribution in various organs after a period of 24 hours. The 50 nm GNPs were accumulated in an overwhelming majority in lungs, besides the 10 nm GNPs showed the most widespread presence in the brain, heart, kidneys, lungs, testis, and thymus (De Jong *et al.* 2008). The concentration of GNPs in the liver was found to be the highest, followed by the spleen. The *in vivo* examinations of nanoparticle distributions performed by Huang *et al.* showed that liver, spleen, kidney and lung are the target organs for gold polygonal (20–50 nm) nanoparticles (Huang *et al.* 2008). The effect of the size of colloidal GNPs was confirmed also in similar work (Sonavane *et al.* 2008), where GNPs with different sizes 15, 50, 100 and 200 nm were applied in mice. Interestingly, they showed that 15 and 50 nm colloidal GNPs are able to pass the blood-brain barrier as evident from gold concentration in the brain.

In another report, the acute toxicity and organ distribution of GNPs were examined (Cho *et al.* 2009). After several different time expositions of 13 nm PEG-coated GNPs, the liver, spleen, kidneys, lungs, brain and testis were examined. In conclusion, 13 nm PEG-coated GNPs were seen to induce acute inflammation and apoptosis in the mouse liver, where their vast accumulation was observed.

Biodistribution and histological studies were performed also, for example, by Terentyuk *et al.* using 15 nm and 50 nm PEG-coated colloidal GNPs and 160 nm silica/gold nanoshells (Terentyuk *et al.* 2009). They determined that their GNPs were mainly accumulated in the spleen and liver 24 hours after injection and the biodistribution was shown to be size dependent.

It was also shown that 20 nm PEG$_{5000}$-coated GNPs exhibit prolonged blood circulation and reduced uptake by the liver and the spleen, while most 80 nm GNPs were rapidly taken up by cells of the reticuloendothelial system (Zhang *et al.* 2009). Biodistribution of 20 nm GNPs in more than 25 organs was examined by Balasubramanian *et al.* at 1 day, 1 week, 1 month and 2 months after a single intravenous injection in rats. Au in this study was rapidly and consistently accumulated in liver and spleen. Two months post-injection GNPs were inefficiently cleared from the body through the urine and faeces (Balasubramanian *et al.* 2010).

Last but not least I would mention a study made in the laboratory of Hodny with cationic GNRs, of which this bachelor work is derived (Zarska *et al.* 2018). Colloid cationic GNRs with dimensions 54 x 25 nm (described in Chapter 1.5) were intravenously applied in mice and the biodistribution was examined 24 h and 10 days in lungs, brain, spleen, small and large intestine and liver. Majority of colloidal GNRs accumulated in the spleen followed by lungs and liver. It should be highlighted that no pathological findings during both 24 hours and a 10-day period were observed in this study.

1.5   MTAB Gold Nanorods

Colloidal GNRs ranging from 2 to 200 nm in diameter have excellent biocompatibility, an amendable method for surface modification and attractive physicochemical properties (mentioned above) as well. The shape and size of the GNRs are determined during synthesis by cetyltrimethylammonium bromide (CTAB), see Chapters 1.1 and Chapter 3.3. CTAB forms a bilayer on the surface of GNRs and because its molecule contains quaternary ammonium group, the GNRs get a positive charge (Nikoobakht and El-Sayed 2001). Colloidal GNRs coated with CTAB are stable only in

solution in equilibrium with a certain concentration of free CTAB. However, CTAB is strongly toxic to the cells and must be removed before biological applications.

Due to commercial availability, it is a very common alternative to use PEG-SH containing thiol group (mentioned in Chapter 1.2), but in our research, cationic GNRs with toxic CTAB molecule was replaced by its non-toxic cationic analogue (16-mercaptohexadecyl) trimethylammonium bromide (MTAB) (Zarska *et al.* 2016). Both chemical compounds are almost identical, except the thiol group in case of MTAB (see Fig. 9).
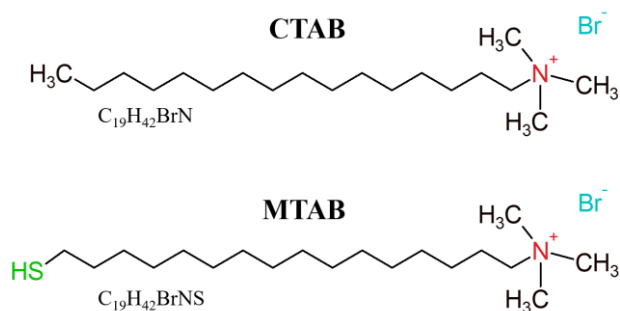

Fig. 9 – The comparison of the two used ligands (by Michal Šrámek).

Vigderman *et al.* (2012) proved with proton nuclear magnetic resonance (^{1}H NMR) analysis, that MTAB is fully able to replace CTAB from GNRs (Vigderman *et al.* 2012) based on a study of Nikoobakht and El-Sayed. They described 9 years earlier that CTAB is noncovalently coated to GNRs, whereas the thiol group of MTAB binds with a stronger electrostatic or covalent bond and a positive charge is still retained (Nikoobakht and El-Sayed 2003). They also stated that CTAB forms a bilayer structure, whereas MTAB forms only a monolayer (Fig. 10).
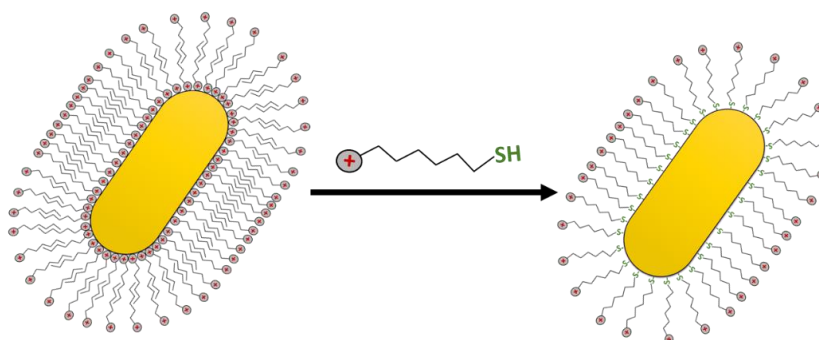

Fig. 10 – Exchange of CTAB bilayer for the MTAB thiol monolayer
(redrawn Figure from Vigderman *et al.* 2012).

These cationic colloidal GNRs modified with MTAB (^{MTAB}GNRs) have a great potential for medical applications including tumour treatment. A tumour itself has

physiological barriers, such as vascularity, heterogeneous blood supply and heterogeneous architecture (Bilensoy 2010). For treatment to be successful, it is very important to overcome these barriers. Properties of colloidal MTABGNRs, such as cellular internalization and stability have been already determined (Zarska *et al.* 2016). Moreover, Zarska *et al.* showed recently, that MTABGNRs have exceptionally high cellular uptake by various cancer cells that makes them a promising tool for tumour treatment (Zarska *et al.* 2016). Cellular uptake of MTABGNRs was described in this study as a two steps process (Zarska *et al.* 2016). First, fast passive adhesion to the cell membrane is mediated by sulphated proteoglycans. The expression of sulphated proteoglycans is the major factor, which depends on cell type. The electrostatic adhesion between cationic MTABGNRs and negatively charged proteoglycans occurs within minutes. The second step is active transmembrane and intracellular transport of individual nanorods via clathrin-mediated endocytosis and of aggregated nanorods via macropinocytosis.

2. Aims of the Bachelor Thesis

- To provide an overview of the field of colloidal AuNPs summarizing their physicochemical and biological features and potential biomedical applications.
- To perform a microscopic examination (light microscope/confocal microscope/scanning electron microscope) of blood after exposure to GNRs with cationic charge mediated by MTAB.
- To compare individual human blood cells according to their interaction rate with ^{MTAB}GNRs.
- To confirm the localization of ^{MTAB}GNRs nanoparticles in mouse spleen tissue after *in vivo* application by histochemistry.

3. Material and Methods

3.1 Chemicals

Tab. 1 – The list of used chemicals.

CHEMICAL	DISTRIBUTOR	CATALOGUE No.
cetyltrimethylammonium bromide (CTAB)	Sigma–Aldrich	H9151–100G
(16–mercaptohexadecyl) trimethylammonium bromide (MTAB)	Chemistry Department, UHK	
D-glucose anhydrous	Penta	12020–31000
ethylenediaminetetraacetic acid (EDTA)	Sigma–Aldrich	E5134–500G
phosphate-buffer saline (PBS)	Media and Glass Washing Department, IMG	
methanol	Sigma–Aldrich	322415-2L
Giemsa stain	Sigma–Aldrich	G4507-5G
4% formaldehyde	VWR	9713.1000
Mowiol 4–88	Sigma–Aldrich	81381
DAPI (4',6–diamidino–2–phenylindole)	Sigma–Aldrich	D9542–5 MG
isopropyl alcohol A.G.	Penta	17510–11000
formaldehyde 20% sol. EM grade	Biogen	15713
glutaraldehyde EM grade 25%	Biogen	16220
ethanol absolute	VWR	1.00983.1000
acetone A.G.	Penta	10060–11000
water for injection	B. Braun Melsungen AG	87/024/98–C
Forane®	AbbVie s.r.o.	05/196/90–C
xylene	VWR	LACH20060AT0M1000
periodic acid	Sigma–Aldrich	P7875
Schiff's reagent	Sigma–Aldrich	1090330500
Mayer's hematoxylin	Sigma–Aldrich	MHS16-500ML
DPX mountant for histology	Sigma–Aldrich	06522
sodium citrate	Sigma–Aldrich	C8532
bovine serum albumin (BSA)	Sigma–Aldrich	A9647_50 G
Hank's balanced salt solution (HBSS)	Media and Glass Washing Department, IMG	

3.2   Antibodies

Tab. 2 – The list of used antibodies.

ANTIBODY	DISTRIBUTOR	CATALOGUE No.
FITC–conjugated anti–CD 41	Beckman Coulter	IM0649U
WGA (wheat germ agglutinin)	Thermo Fisher Scientific	W11261

3.3   Synthesis

3.3.1   Gold Nanorods

Colloidal GNRs (54 x 25 nm) were synthesized according to the protocol described previously (Zarska *et al.* 2016) using seed-mediated growth (see Chapter 1.5) as demonstrated by El-Sayed groups (Nikoobakht and El-Sayed 2003) and Murphy (Busbee *et al.* 2003). GNRs concentration during the reactions was determined by monitoring the optical absorbance of solutions at 390 nm as described previously (Edgar *et al.* 2012) and was expressed as a molar amount of metallic gold (Au^0) in colloid solution using the formula:

$$Au^0[\mu M] = \frac{A_{390}}{path\ length\ [cm]} \times 355$$

Synthesized CTAB-stabilized GNRs have absorption maximum spectrally tuned to 633 nm of the electromagnetic spectrum for detection by microscopy or to the red region (800 nm) for thermotherapy, which is as a part of NIR light (above in Fig. 4).

3.3.2   MTAB

The synthesis of (16–mercaptohexadecyl)trimethylammonium bromide (MTAB) was performed according to Zubarev group (Vigderman *et al.* 2012) and adapted for higher yield according to Zarska *et al.* (2016).

3.3.3   Ligand Exchange

Ligand exchange of CTAB for MTAB was performed according to Vigderman *et al.* (2012) as described in detail in Zarska *et al.* (2016). The cross-section of this molecule is small enough to form a compact monolayer on the surface of nanorods (Fig. 10), thus providing their solution stability (see Chapter 1.5).
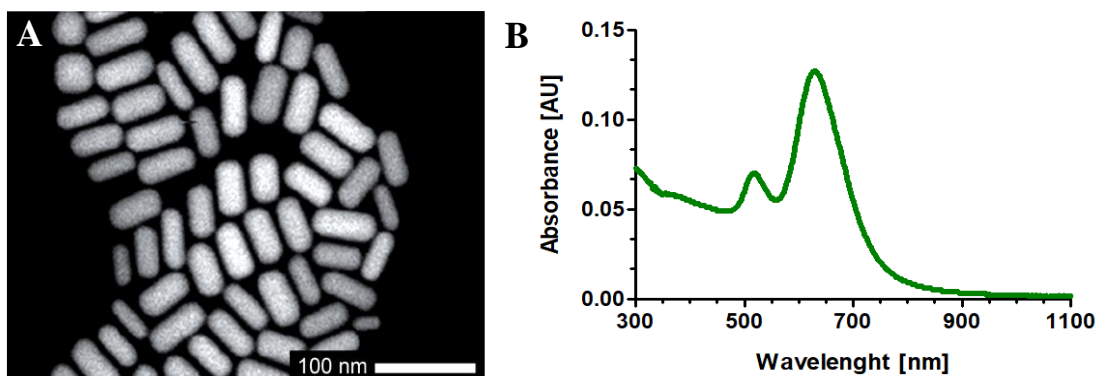
Fig. 11 – (A) FE–SEM images of ^{MTAB}GNRs with longitudinal LSPR tuned to 633 nm (Zarska *et al.* 2016). (B) The spectrum of ^{MTAB}GNRs (by Michal Šrámek).

The uniform (monodisperse) shape of our ^{MTAB}GNRs is evident (Fig. 11-A), as detected by the FE–SEM analysis. Absorption spectrum (Fig. 11-B) estimated after functionalization of nanoparticles with MTAB contains both transversal and longitudinal LSPR confirming nanorods shape (see Chapter 1.1 and Fig. 4) and their good stability.

3.4   Exposure of Human Blood to ^{MTAB}GNRs

The blood from a healthy volunteer (*Homo sapiens sapiens*, male, 27 years old, blood type 0+) was drawn into 15 mL tube without the use of anticoagulants (as reasoned in Chapter 5). To 1 mL of blood 0.5 mL 500 µM ^{MTAB}GNRs in 5% glucose and 1 mL 2 mM EDTA, 1x PBS (pH = 7.2) was added. Blood was incubated with nanorods at room temperature for 5 hours hold at very slow agitation. Then the microscopic examinations of samples were performed (Section 3.4.1).

3.4.1   Preparation and Microscopy Examinations of Blood Smears

After blood collection and incubation with ^{MTAB}GNRs, blood smears were prepared with a drop of blood and air-dried.

a)   <u>For light microscopy imaging:</u>

Blood smears on Superfrost Plus slides were fixed with absolute methanol in Coplin jar for 5 minutes at room temperature and then stained with Giemsa (diluted 1:20 in 1x PBS) for 20 minutes. After twice washing with 1x PBS, the smears were let to dry well in the air. The bright-field images of blood cells were captured by a Leica DM6000 B microscope (with a Leica DFC490 colour camera).

b)   <u>For confocal microscopy imaging</u>

Blood smears on Superfrost Plus slides were fixed with fixative solution (5 mL of 4% formaldehyde and 45 mL of 96% ethanol) in Coplin jar at room temperature for 5 minutes. The glass slides were then washed with 1x PBS and platelets were stained

with FITC anti–CD41 antibody (diluted 1:10 in 1x PBS) for 1 hour. After washing with 1x PBS the samples were mounted to coverslips using Mowiol 4–88 containing DAPI and scanned by confocal microscopy (Leica TCS SP8 AOBS confocal microscope, 633 nm excitation laser, the detection window 631 – 636 nm) using reflectance as described by Zarska *et al.* (2016). 405 nm laser was used to excite DAPI (emission 445–485 nm) and 498 nm laser to excite FITC anti–CD41 (emission 510–560 nm).

   c)   <u>For field emission scanning–electron microscopy:</u>

The silicon wafers (sample holders) were degreased with isopropanol, washed by 70% ethanol and air-dried in sterile conditions. Then they were inserted into 12–well plate and rinsed with 1x PBS. In next step, the drops of blood were gently transferred onto silicon wafers following modified human blood cells protocol (Müeller, 2016) available on the website of Leica Microsystems and left at 25 °C for 5 minutes. Fixation was performed with 4% formaldehyde, 0.4% glutaraldehyde in 1x PBS (pH = 7.2) at room temperature for 1 hour. The silicon wafers were then washed 3 times with 1x PBS and dehydrated in ethanol series (30%, 50%, 70%, 80%, 90%, 96%, 100% for 10 minutes each), immersed in absolute acetone for 10 minutes and finally air-dried. The images were captured by FE–SEM (JEOL JSM–7500 F; JEOL, Tokyo, Japan). Backscattered electron images were acquired at acceleration voltage 15 kV.

3.5   *Mouse Animal Model*

Mouse C57/BL6 (*Mus musculus*, male, 12-13 weeks old) was obtained from Charles River Laboratories (Sulzfeld, Germany) and bred in the animal facility of the Institute of Molecular Genetics of the ASCR, v. v. i., Prague, Czech Republic. The experimental protocol was approved by the Institutional Animal Care Committee of the Institute of Molecular Genetics of the ASCR, v. v. i., Prague and by the Departmental Expert Committee for the Approval of Projects of Experiments on Animals of the Czech Academy of Sciences, Prague.

3.5.1   *In vivo Application of Gold Nanoparticles*

Freshly prepared [MTAB]GNRs were centrifuged at 6000 x g for 10 minutes and resuspended in 5% glucose/water solution to obtain 0.35 mM Au^0 of [MTAB]GNRs. Next, 150 µl of [MTAB]GNRs (corresponding to 10 µg Au/mouse = 0.37 mg [MTAB]GNRs/kg of body weight) was injected intravenously via retro-orbital sinus to C57/BL6 mouse (under short-term isoflurane anaesthesia). The mouse was sacrificed 24 hours later. Spleen was collected immediately and sliced into $0.3 – 0.8 \text{ cm}^3$ pieces, which were fixed in 4%

formaldehyde at 4 °C for 24 hours before further histochemical analysis (see Section 3.5.2).

3.5.2 Histochemistry

Fixed tissues were washed twice in water, transferred into 70% ethanol and incubated for 24 hours, and then the washing step was repeated once again. Next, the samples in 70% ethanol were processed using an ASP200 tissue processor (Leica Microsystems) and subsequently embedded in paraffin wax using an EG1150 embedding station (Leica Microsystems). Paraffin blocks were cut into 4 mm slices, which were then transferred onto Superfrost Plus slides (Thermo Fisher Scientific) and dried at 37 °C overnight. Tissue sections were then dewaxed in xylene for 2 - 10 minutes, hydrated in descending series of ethanol/water (100%, 96%, 70%, 50% for 3 minutes each) and finally rinsed in distilled water for 5 minutes.

a) <u>For light microscopy imaging:</u>

The dewaxed and hydrated tissue sections on the slides were soaked in 0.5% periodic acid for 5 minutes, carefully washed with distilled water and stained by Schiff's reagent at room temperature for 15 minutes. Then the slides were washed with running tap water and counterstained in Mayer's hematoxylin solution at room temperature for 3 minutes. Washed slides were dehydrated in ethanol series (50%, 70%, 96%, 100% for 3 minutes each), air-dried and mounted with DPX mounting medium. Bright-field images were acquired by a Leica DM6000 B microscope equipped with a Leica DFC490 colour camera.

b) <u>For confocal microscopy imaging:</u>

Tissue slices were boiled in 0.01 M sodium citrate (pH = 6.0) in an electric pressure pot for 12 minutes and blocked with 3% BSA at room temperature for 30 minutes. To visualize cell membranes WGA-Alexa Fluor 488 conjugate was used at concentration 5 mg/mL in HBSS at 37 °C for 1 hour. The sections were then washed 3 times with 1x PBS and covered with coverslips using Mowiol 4–88 containing DAPI. [MTAB]GNRs in tissues were detected by confocal reflectance microscopy (Leica TCS SP8 AOBS confocal microscope, 633 nm excitation laser, the detection window 631–636 nm) as described by Zarska *et al.* (2016). 405 nm laser was used to excite DAPI (emission 445–485 nm) and 498 nm laser to excite Alexa Fluor 488 (emission 510–560 nm).

4. Results

4.1 Blood Interaction

The blood volunteer male's human blood type 0+ was used to determine the interaction of blood components with GNRs bearing biocompatible cationic MTAB. Experiments were performed in the presence of EDTA as an anticoagulant (related to Chapter 3.4 and explained in Chapter 5).

To examine changes in the blood, the light microscopy was made first. The interaction of ^{MTAB}GNRs (100 mM Au^0) with human blood was detected using confocal imaging with AOBS system and then confirmed by FE-SEM. The results *in vitro* showed that a very small amount of ^{MTAB}GNRs interacted with the cell membrane of RBCs (Fig. 12). Interestingly, RBCs preserved their shape and no lysis was observed.
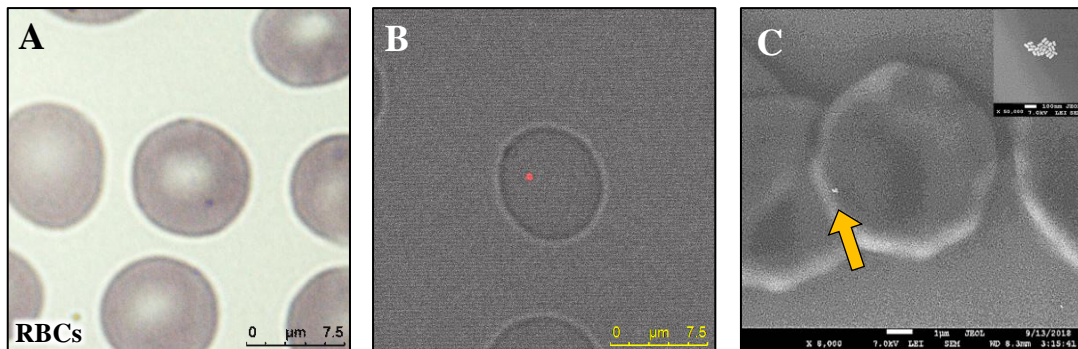

Fig. 12 – Interaction of RBCs with ^{MTAB}GNRs. (A) Giemsa stain. (B) Confocal image of ^{MTAB}GNRs. (C) FE–SEM image.

The marked interaction of ^{MTAB}GNRs with polymorphonuclear WBCs (granulocytes) was detected (Fig. 13). All granulocytes possess homogenous, similar extent of interaction with ^{MTAB}GNRs.

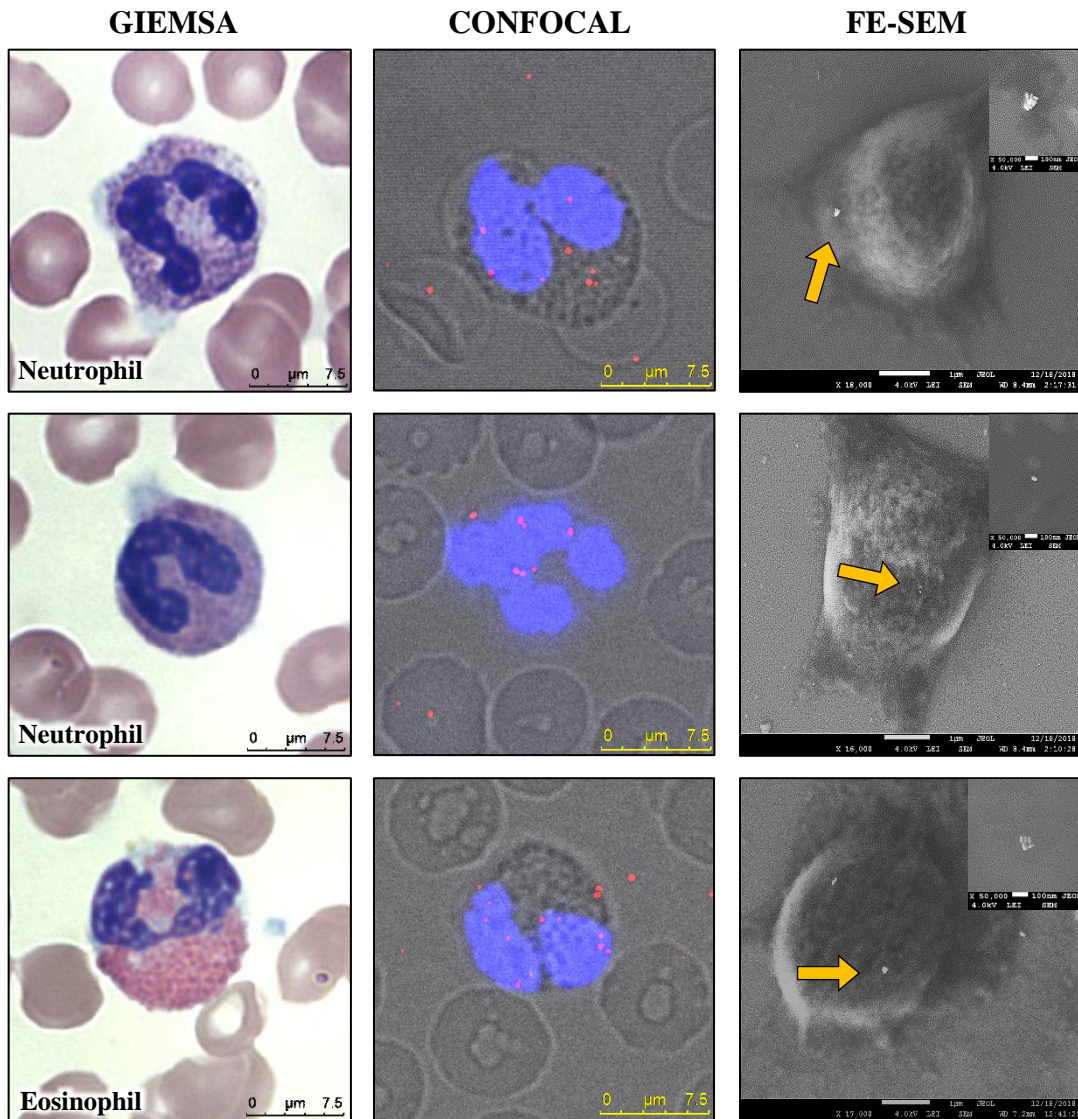| GIEMSA	CONFOCAL	FE-SEM

Fig. 13 – The set of interactions of polymorphonuclear granulocytes (WBCs), nuclei stained by DAPI with ^{MTAB}GNRs.

While granulocytes possess a homogenous mode of interaction (Fig. 13), monomorphonuclear agranulocytes (WBCs) show rather aggregates after interaction (Fig. 14). Blast cells are not typically found in the circulating blood of healthy individuals. Therefore, their interaction and presence could be slightly ignored.
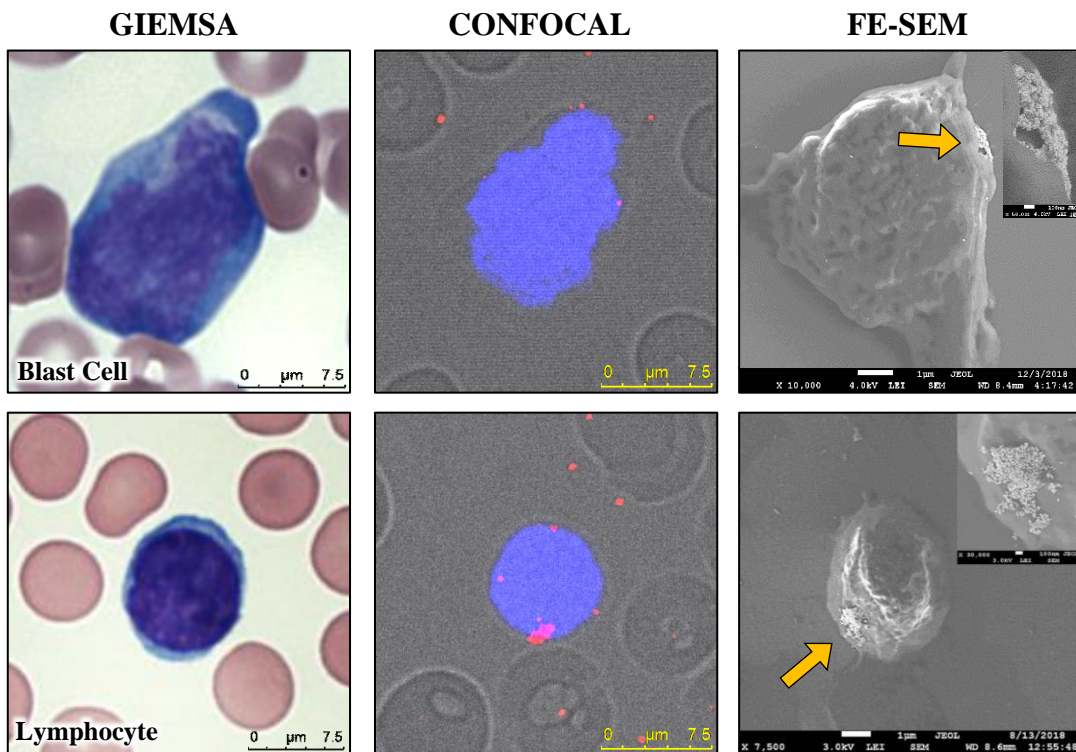

Fig. 14 – The set of interactions of monomorphonuclear agranulocytes (WBCs) nuclei stained by **DAPI** with **MTABGNRs**.

Notably, the extensive interaction of MTABGNRs was observed with anuclear objects positive for blood thrombocyte marker CD41 (Fig. 15).
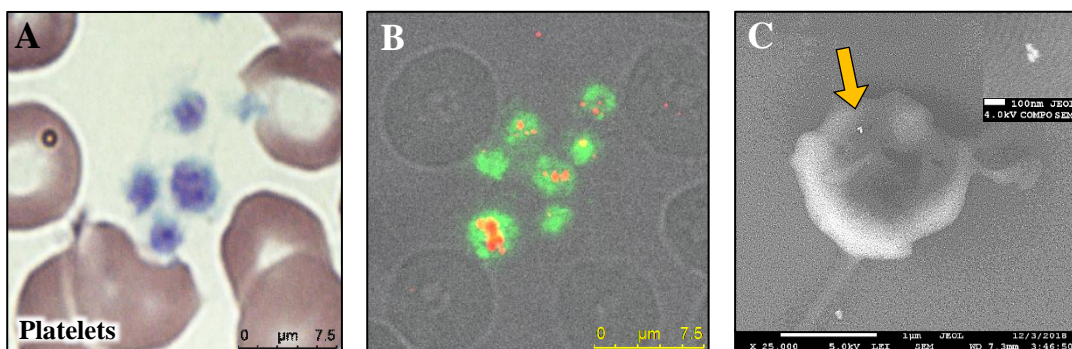

Fig. 15 – Interaction of platelets with MTABGNRs. (A) Giemsa stain. (B) Confocal image of **CD41** positive platelets with **MTABGNRs**. (C) FE–SEM image.

4.2 Distribution of ^{MTAB}GNRs in vivo

To determine organ biodistribution of ^{MTAB}GNRs, the mouse was chosen as a model organism. After intravenous administration of ^{MTAB}GNRs (10 µg Au/mouse), the accumulation of ^{MTAB}GNRs was detected using confocal imaging with AOBS system. The results showed ^{MTAB}GNRs accumulated in the spleen. No pathological findings were observed after staining spleen histochemically (Fig. 16).
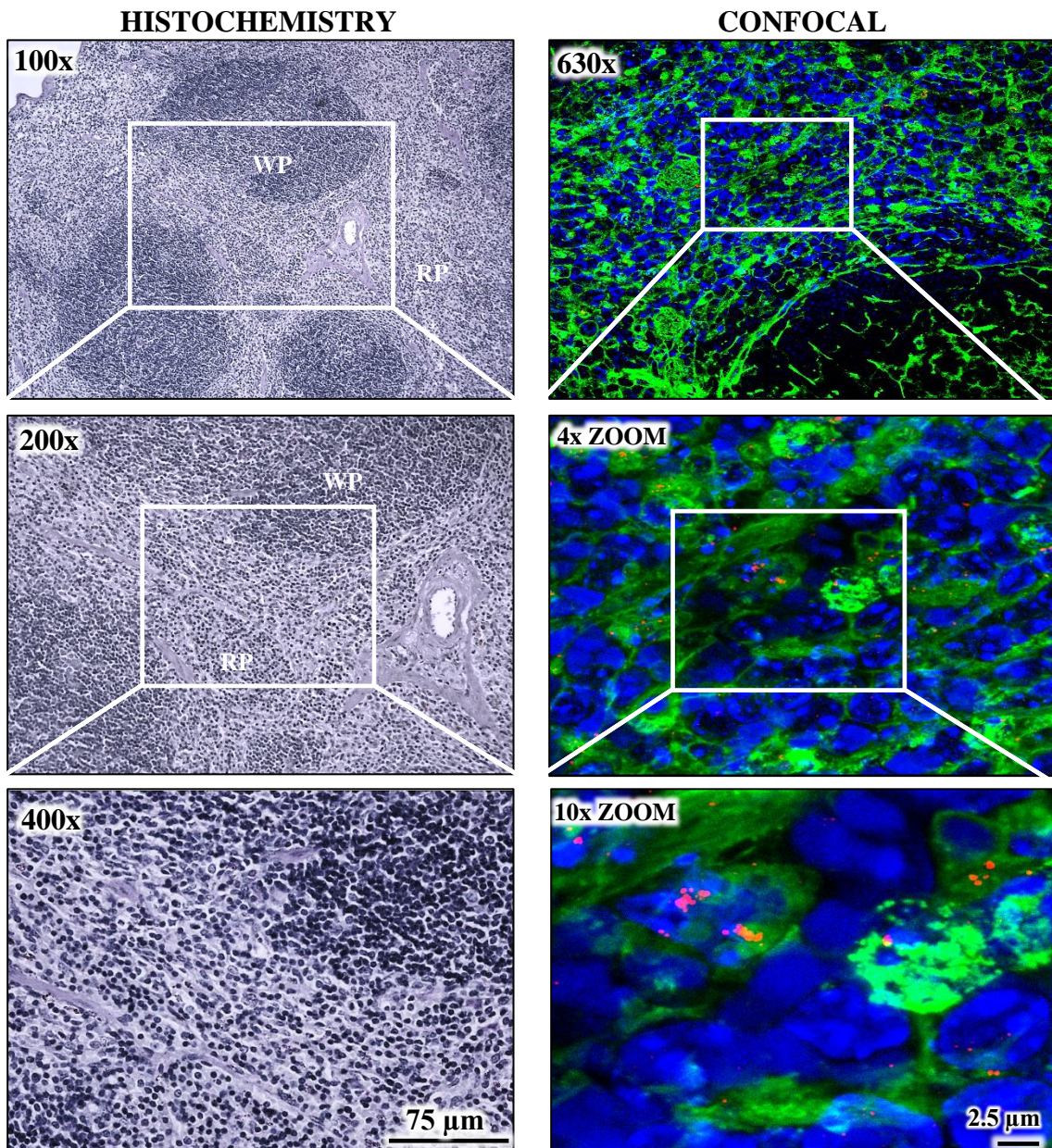
HISTOCHEMISTRY **CONFOCAL**

Fig. 16 – Accumulation of ^{MTAB}GNRs in the mouse spleen. Histochemistry – distinguishable red (RP) and white pulp (WP). Confocal microscopy - cells membrane-specific staining was done with **WGA**, nuclei by **DAPI** + detection of ^{MTAB}**GNRs**.

5. Discussion

5.1 Influence of Heparin on ^{MTAB}GNRs

In Section 1.4.2 is described briefly coating of bloodstream plasma protein to the GNPs and in earlier experiments, we demonstrated a similar function of heparin. Due to his negatively charged sulphate, heparin binds strongly on cationic ^{MTAB}GNRs and acts like serum proteins, thus there is strong interaction between ^{MTAB}GNRs and sulphated proteoglycans (Zarska *et al.* 2016). As a result, the aggregation of thrombocytes isolated from heparinized ^{MTAB}GNRs-blood mixture was visible. We already know that the aggregation of nonactivated or activated thrombocytes isolated from EDTA-laden blood was not observed in the presence of ^{MTAB}GNRs. Therefore, EDTA was used as an anticoagulant (related to Chapter 3.4 and mentioned in Chapter 4.1).

5.2 The Rate of Interaction Between ^{MTAB}GNRs and Blood Cells

The immune cells interact with ^{MTAB}GNRs more efficiently than RBCs (Fig. 13 and Fig. 14) probably either through receptor-mediated endocytosis or through reduction of the coulombic repulsion between the particles and negatively charged cell membranes. The proteins that bind nanoscale particles, such as polymeric nanoparticles, iron–oxide particles, liposomes, and carbon nanotubes have been examined before (Dobrovolskaia *et al.*, 2009). Already published studies show that albumin, apolipoprotein, immunoglobulins, complement, and fibrinogen are the most abundant species bound to gold colloids (see Section 1.4.2). Study of Zarska *et al*. corresponds also to Section 1.4.2 and our study (Zarska *et al.* 2016) where BSA is described to have an influence on the stability of ^{MTAB}GNRs, but what is important, also on the cellular uptake.

5.3 Microscopy for Cell Differentiation

Microscopy examination of blood smears stained with Giemsa allowed me to recognize individual blood cells. RBCs are the most represented, without a nucleus and have a pink colour. Polymorphonuclear WBCs can be nicely distinguished from monomorphonuclear WBCs thanks to nuclei with multiple lobes (see Section 1.4.1.2) and granules in the cytoplasm (eosinophils - pink cytoplasm and red to orange granules, basophils - blue coarse granules). Platelets are visible as smaller structures with violet to purple colour with no nucleus (Dean 2005). However, under ordinary light microscopy, the absorption of ^{MTAB}GNRs on the surface of each blood cell is undetectable. Thus, we used confocal microscopy with AOBS system as a primary and simplest method to detect

^{MTAB}GNRs (see Chapter 4.1). Due to co-staining with DAPI, it is possible to recognize morphology of nuclei and thus to allow differentiation of cells to polymorphonuclear (granulocytes) and monomorphonuclear (agranulocytes), as can be seen in Fig. 13 and Fig. 14. Still, without using any specific fluorescent antibodies against cellular cluster of designation (CD), it is not possible conclusively to differentiate the exact type of WBCs (except the case of platelets – Fig. 15, where fluorescent antibody against CD41+ was used) and compare them with blood cells stained with Giemsa, only rough estimation is possible based on cells size and stained nuclei shape. The same applies to FE-SEM.

5.4   Cell Damage and Toxic Effects

Importantly, the RBCs after interaction with ^{MTAB}GNRs did not show any lysis or visible damage (Fig. 12). Zarska *et al.* also confirmed no damage of WBCs and no lysis of RBCs after exposure of ^{MTAB}GNRs (Zarska *et al.*, 2018). Damage and viability after the exposition of GNRs were examined and published by Paino *et al*. In their study after incubation of peripheral blood mononuclear cells (PBMCs) with citrate modified GNPs (^{CITRATE}GNPs), the cell viability of PBMCs decreased significantly when compared to negative control. Paino *et al.* also investigated the DNA damage caused by ^{CITRATE}GNPs by comet assay. They depict the extensive damage to DNA after the exposition of PBMCs to ^{CITRATE}GNPs, compared to negative control (Paino *et al.* 2012). This study practically shows that it is necessary to take also the ligand-functionalization for consideration (as already mentioned in Chapter 1.2).

Importantly, no acute toxic effects of ^{MTAB}GNRs was found. High accumulation of applied 10 µg (corresponding to 0.37 mg ^{MTAB}GNRs/kg of body weight) of gold per mouse showed no pathological changes in mouse spleen (Fig. 16). That indicates the good tolerance of ^{MTAB}GNRs by living systems, which is promising for future applications. Given the good organism tolerance is not always obvious. It was found, that the smaller GNPs (2–4 nm and 5–7 nm) induced serious toxic effect as it is easier to be taken up into cells and to exert damage to them (Jia *et al.* 2017). This type of GNPs can catalyse NO production in blood and eventually result in cell necrosis or apoptosis.

5.5   Proper Functionalization

Functionalization has a significant effect on circulation time and localization of GNPs. In our experimental settings, we estimated significant ^{MTAB}GNRs accumulation in the mouse spleen mainly due WBCs and platelets, because they are known to be removed

by the spleen macrophages (see Section 1.4.1.1 and Section 1.4.1.2). Moreover, Zarska *et al.* showed that small amounts of [MTAB]GNRs were found also in the lungs and liver and the final gold content in the spleen, lungs and liver was quantified by ICP–MS. The highest gold concentration after 24 hours was measured in the spleen, whereas in the lungs and liver the concentration was lower. Both single and clustered [MTAB]GNRs in the spleen examined by FE–SEM analysis confirmed this statement (Zarska *et al.*, 2018). In different experimental settings with PEG-SH modified GNRs (Chapter 1.2 and Section 1.4.3) was shown enhanced circulation time of these GNRs compared to the 'modified' GNRs by CTAB ([CTAB]GNRs). Niidome *et al.* found that after 30 minutes from the intravenous injection, [CTAB]GNRs were cleared from the circulation, and went to the liver, whereas 54% of the PEG-SH coated GNRs was found still in the blood (Niidome *et al.* 2006). In a separate study, Akiyama *et al.* showed that the density of the PEG molecules on the GNRs surface is very important to avoid non-specific uptake by the reticuloendothelial system and thus to gain longer circulation times (Akiyama *et al.* 2009).

5.6   Future Steps

I consider thereby as substantial to study blood cell-GNPs interactions for a closer understanding organism's blood circulation of the nanoparticles in general and estimation of their biodistribution. Recent evidence shows that functionalization with a correct biocompatible molecule (in Chapter 1.2) has a pivotal role in protein corona formation (in Section 1.4.2) and finally in interaction with blood cells (Section 1.4.1.2).

In the case of a more detailed study of this phenomenon, I would suggest extending this study with the examination of GNRs interaction with different blood types. The blood type is determined by antigens on the surface of red blood cells as well as the Rh system (and other systems). These antigens may be proteins, carbohydrates, glycoproteins, or glycolipids, depending on the blood group system (Dean 2005). In the bloodstream, such proteoglycans of the blood cells could bind the positively charged colloid GNPs and thus facilitate their interaction with the RBCs. It should be noted, that not only interaction but also biodistribution could be influenced by different blood types. The understanding of the mechanism of interaction of [MTAB]GNRs with blood cells and their tissue distribution after the systemic application is clearly fundamental for future clinical research, including cancer therapy.

Another future step could be using flow cytometry for immunophenotyping of blood cells. Flow cytometry allows us to differentiate the exact type of WBCs and could serve as an additional method for microscopy. Commonly used CD molecules are listed in Tab. 4 in the attachments.

Lastly, I would point out that the photothermal properties of gold nanomaterials are particularly attractive as an approach to treat diseased cells or tissues if the correct surface targeting will be achieved. There is a clear need to perform careful studies of their longer-term impacts both on human and environmental health.

6. Conclusion

The aims of my bachelor thesis were to examine and compare the interaction rates of ^{MTAB}GNRs with individual human blood cells and confirm the localization of ^{MTAB}GNRs in mouse spleen. In the experimental part, my tasks were to handle basic nano research and also molecular biology methods in Laboratory of Genome Integrity of Institute of Molecular Genetics of the ASCR, v. v. i., such as proper isolation and treatment of human peripheral blood, blood staining, histology and microscopic observations.

At the beginning of the bachelor thesis, I demonstrated the current information about various types of GNPs, their possible use and proposed that specific ^{MTAB}GNRs were delivered to the spleen by absorption primarily by specific types of blood cells.

Description of different ways of the interactions and tissue distributions after the systemic application is clearly fundamental for future clinical utilization of GNPs, including cancer therapy. The obtained data are part of scientific publications and presented at conferences.

7. References

1) AILLON, Kristin L., Yumei XIE, Nashwa EL-GENDY, Cory J. BERKLAND and M. Laird FORREST, 2009. Effects of nanomaterial physicochemical properties on *in vivo* toxicity. *Advanced Drug Delivery Reviews*. **61**(6), 457–466. ISSN 0169409X. DOI: 10.1016/j.addr.2009.03.010

2) AKIYAMA, Yasuyuki, Takeshi MORI, Yoshiki KATAYAMA and Takuro NIIDOME, 2009. The effects of PEG grafting level and injection dose on gold nanorod biodistribution in the tumor-bearing mice. *Journal of Controlled Release*. **139**(1), 81–84. ISSN 01683659. DOI: 10.1016/j.jconrel.2009.06.006

3) ALKILANY, Alaaldin M., Lucas B. THOMPSON, Stefano P. BOULOS, Patrick N. SISCO and Catherine J. MURPHY, 2012. Gold nanorods: Their potential for photothermal therapeutics and drug delivery, tempered by the complexity of their biological interactions. *Advanced Drug Delivery Reviews*. **64**(2), 190–199. ISSN 0169409X. DOI: 10.1016/j.addr.2011.03.005

4) BALASUBRAMANIAN, Suresh K., Jinatta JITTIWAT, Jayapal MANIKANDAN, Choon-Nam ONG, Liya E. YU and Wei-Yi ONG, 2010. Biodistribution of gold nanoparticles and gene expression changes in the liver and spleen after intravenous administration in rats. *Biomaterials*. **31**(8), 2034–2042. ISSN 01429612. DOI: 10.1016/j.biomaterials.2009.11.079

5) BALOGH, Lajos, Shraddha S. NIGAVEKAR, Bindu M. NAIR, Wojciech LESNIAK, Chunxin ZHANG, Lok Yun SUNG, Muhammed S.T. KARIAPPER, Areej EL-JAWAHRI, Mikel LLANES, Brian BOLTON, Fatema MAMOU, Wei TAN, Alan HUTSON, Leah MINC and Mohamed K. KHAN, 2007. Significant effect of size on the *in vivo* biodistribution of gold composite nanodevices in mouse tumor models. *Nanomedicine: Nanotechnology, Biology and Medicine*. **3**(4), 281–296. ISSN 15499634. DOI: 10.1016/j.nano.2007.09.001

6) BERGEN, Jamie M., Horst A. VON RECUM, Thomas T. GOODMAN, Archna P. MASSEY and Suzie H. PUN, 2006. Gold Nanoparticles as a Versatile Platform for Optimizing Physicochemical Parameters for Targeted Drug Delivery. *Macromolecular Bioscience*. **6**(7), 506–516. ISSN 1616-5187. DOI: 10.1002/mabi.200600075

7) BILENSOY, Erem, 2010. Cationic nanoparticles for cancer therapy. *Expert Opinion on Drug Delivery*. **7**(7), 795–809. ISSN 1742-5247. DOI: 10.1517/17425247.2010.485983

8) BUSBEE, Brantley D., Sherine O. OBARE and Cantherine J. MURPHY, 2003. An Improved Synthesis of High-Aspect-Ratio Gold Nanorods. *Advanced Materials*. **15**(5), 414–416. ISSN 09359648. DOI: 10.1002/adma.200390095

9) CHARD, Thomas, 1992. Pregnancy tests: a review. *Human Reproduction (Oxford, England)*. **7**(5), 701–710. ISSN 0268-1161.

10) DE JONG, Wim H., Werner I. HAGENS, Petra KRYSTEK, Marina C. BURGER, Adriënne J.A.M. SIPS and Robert E. GEERTSMA, 2008. Particle size-dependent organ distribution of gold nanoparticles after intravenous administration. *Biomaterials*. **29**(12), 1912–1919. ISSN 01429612. DOI: 10.1016/j.biomaterials.2007.12.037

11) DEAN, Laura, 2005. Blood Groups and Red Cell Antigens. *Bethesda (MD): National Center for Biotechnology Information (US)*. 98. Available from: https://d360prx.biomed.cas.cz:2469/books/NBK2263/

12) DOBROVOLSKAIA, Marina A., Anil K. PATRI, Jiwen ZHENG, Jeffrey D. CLOGSTON, Nader AYUB, Parag AGGARWAL, Barry W. NEUN, Jennifer B. HALL and Scott E. MCNEIL, 2009. Interaction of colloidal gold nanoparticles with human blood: effects on particle size and analysis of plasma protein binding profiles. *Nanomedicine: Nanotechnology, Biology and Medicine*. **5**(2), 106–117. ISSN 15499634. DOI: 10.1016/j.nano.2008.08.001

13) DREADEN, Erik C., Alaaldin M. ALKILANY, Xiaohua HUANG, Catherine J. MURPHY and Mostafa A. EL-SAYED, 2012. The golden age: gold nanoparticles for biomedicine. *Chem. Soc. Rev*. **41**(7), 2740–2779. ISSN 0306-0012. DOI: 10.1039/C1CS15237H

14) EDGAR, Jonathan A., Andrew M. MCDONAGH and Michael B. CORTIE, 2012. Formation of Gold Nanorods by a Stochastic "Popcorn" Mechanism. *ACS Nano*. **6**(2), 1116–1125. ISSN 1936-0851. DOI: 10.1021/nn203586j

15) EUSTIS, Susie and Mostafa A. EL-SAYED, 2006. Why gold nanoparticles are more precious than pretty gold: Noble metal surface plasmon resonance and its enhancement of the radiative and nonradiative properties of nanocrystals of different shapes. *Chem. Soc. Rev.* **35**(3), 209–217. ISSN 0306-0012. DOI: 10.1039/B514191E

16) FAULK, Page W. and Malcolm G. TAYLOR, 1971. Communication to the editors. *Immunochemistry.* **8**(11), 1081–1083. ISSN 00192791. DOI: 10.1016/0019-2791(71)90496-4

17) FLEISCHER, Candace C. and Christine K. PAYNE, 2014. Nanoparticle–Cell Interactions: Molecular Structure of the Protein Corona and Cellular Outcomes. *Accounts of Chemical Research.* **47**(8), 2651–2659. ISSN 0001-4842. DOI: 10.1021/ar500190q

18) HAINFELD, James F., Daniel N. SLATKIN, Thomas M. FOCELLA and Henry M. SMILOWITZ, 2006. Gold nanoparticles: a new X-ray contrast agent. *The British Journal of Radiology.* **79**(939), 248–253. ISSN 0007-1285. DOI: 10.1259/bjr/13169882

19) HAINFELD, James F., Daniel N. SLATKIN and Henry M. SMILOWITZ, 2004. The use of gold nanoparticles to enhance radiotherapy in mice. *Physics in Medicine and Biology.* **49**(18), N309-315. ISSN 0031-9155.

20) HIRSCH, Leon R., Richard J. STAFFORD, James A. BANKSON, Scott R. SERSHEN, Beverly RIVERA, Roger E. PRICE, John D. HAZLE, Naomi J. HALAS and Jennifer L. WEST, 2003. Nanoshell-mediated near-infrared thermal therapy of tumors under magnetic resonance guidance. *Proceedings of the National Academy of Sciences.* **100**(23), 13549–13554. ISSN 0027-8424. DOI: 10.1073/pnas.2232479100

21) HONARY, Soheyla and Foruhe ZAHIR, 2013. Effect of Zeta Potential on the Properties of Nano-Drug Delivery Systems - A Review (Part 1). Tropical Journal of Pharmaceutical Research. 12(2). ISSN 1596-9827. DOI: 10.4314/tjpr.v12i2.19

22) HOREJSI, Vaclav and Jirina BARTUNKOVA, 2005. *Základy imunologie.* Praha: Triton. ISBN 978-80-7254-686-2.

23) HUANG, Xiaohua, Svetlana NERETINA and Mostafa A. EL-SAYED, 2009. Gold Nanorods: From Synthesis and Properties to Biological and Biomedical Applications. *Advanced Materials*. **21**(48), 4880–4910. ISSN 09359648. DOI: 10.1002/adma.200802789

24) HUANG, Xiao-Li, Bin ZHANG, Lei REN, She-Fang YE, Li-Ping SUN, Qi-Qing ZHANG, Mei-Chee TAN and Gan-Moog CHOW, 2008. *In vivo* toxic studies and biodistribution of near infrared sensitive Au–Au2S nanoparticles as potential drug delivery carriers. *Journal of Materials Science: Materials in Medicine*. **19**(7), 2581–2588. ISSN 0957-4530. DOI: 10.1007/s10856-007-3210-7

25) CHITHRANI, Devika B., Arezou A. GHAZANI and Warren C. W. CHAN, 2006. Determining the Size and Shape Dependence of Gold Nanoparticle Uptake into Mammalian Cells. *Nano Letters*. **6**(4), 662–668. ISSN 1530-6984. DOI: 10.1021/nl052396o

26) CHO, Wan-Seob, Minjung CHO, Jinyoung JEONG, Mina CHOI, Hea-Young CHO, Beom Seok HAN, Sheen Hee KIM, Hyoung Ook KIM, Yong Taik LIM, Bong Hyun CHUNG and Jayoung JEONG, 2009. Acute toxicity and pharmacokinetics of 13 nm-sized PEG-coated gold nanoparticles. *Toxicology and Applied Pharmacology*. **236**(1), 16–24. ISSN 0041008X. DOI: 10.1016/j.taap.2008.12.023

27) JAIN, Prashant K., Kyeong Seok LEE, Ivan H. EL-SAYED and Mostafa A. EL-SAYED, 2006. Calculated Absorption and Scattering Properties of Gold Nanoparticles of Different Size, Shape, and Composition: Applications in Biological Imaging and Biomedicine. *The Journal of Physical Chemistry B*. **110**(14), 7238–7248. ISSN 1520-6106. DOI: 10.1021/jp057170o

28) JIA, Yan-Peng, Bu-Yun MA, Xia-Wei WEI and Zhi-Yong QIAN, 2017. The *in vitro* and *in vivo* toxicity of gold nanoparticles. *Chinese Chemical Letters*. **28**(4), 691–702. ISSN 10018417. DOI: 10.1016/j.cclet.2017.01.021

29) KHLEBTSOV, Nikolai and Lev DYKMAN, 2011. Biodistribution and toxicity of engineered gold nanoparticles: a review of *in vitro* and *in vivo* studies. *Chem. Soc. Rev*. **40**(3), 1647–167. ISSN 0306-0012. DOI: 10.1039/C0CS00018C

30) KLEIN, Sabine, Svea PETERSEN, Ulrike TAYLOR, Detlef RATH and Stephan BARCIKOWSKI, 2010. Quantitative visualization of colloidal and intracellular gold nanoparticles by confocal microscopy. *Journal of Biomedical Optics*. **15**(3), 036015. ISSN 10833668. DOI: 10.1117/1.3461170

31) LU, Xianmao, Leslie AU, Joseph MCLELLAN, Zhi-Yuan LI, Manuel MARQUEZ and Younan XIA, 2007. Fabrication of Cubic Nanocages and Nanoframes by Dealloying Au/Ag Alloy Nanoboxes with an Aqueous Etchant Based on $Fe(NO_3)_3$ or NH_4OH. *Nano Letters*. **7**(6), 1764–1769. ISSN 1530-6984. DOI: 10.1021/nl070838l

32) MATON, Anthea and Inc PRENTICE-HALL, 1993. *Human biology and health.* Englewood Cliffs, N.J.: Prentice Hall. ISBN 978-0-13-225491-5.

33) MCNEIL, Scott E., 2005. Nanotechnology for the biologist. *Journal of Leukocyte Biology*. **78**(3), 585–594. ISSN 07415400. DOI: 10.1189/jlb.0205074

34) MOGHIMI, Moein S. and Janos SZEBENI, 2003. Stealth liposomes and long circulating nanoparticles: critical issues in pharmacokinetics, opsonization and protein-binding properties. *Progress in Lipid Research*. **42**(6), 463–478. ISSN 0163-7827.

35) MÜELLER, Wally H., 2016. *Application Note - Human Blood Cells Protocol related instrument Leica EM CPD300*. 2016. B.m.: Leica MICROSYSTEMS. Available from: https://www.leica-microsystems.com/science-lab/human-blood-cells-protocol/

36) NIIDOME, Takuro, Masato YAMAGATA, Yuri OKAMOTO, Yasuyuki AKIYAMA, Hironobu TAKAHASHI, Takahito KAWANO, Yoshiki KATAYAMA and Yasuro NIIDOME, 2006. PEG-modified gold nanorods with a stealth character for *in vivo* applications. *Journal of Controlled Release*. **114**(3), 343–347. ISSN 01683659. DOI: 10.1016/j.jconrel.2006.06.017

37) NIKOOBAKHT, Babak and Mostafa A. EL-SAYED, 2001. Evidence for Bilayer Assembly of Cationic Surfactants on the Surface of Gold Nanorods. *Langmuir*. **17**(20), 6368–6374. ISSN 0743-7463. DOI: 10.1021/la010530o

38) NIKOOBAKHT, Babak and Mostafa A. EL-SAYED, 2003. Preparation and Growth Mechanism of Gold Nanorods (NRs) Using Seed-Mediated Growth Method. *Chemistry of Materials*. **15**(10), 1957–1962. ISSN 0897-4756. DOI: 10.1021/cm020732l

39) PACIOTTI, Giulio F., Lonnie MYER, David WEINREICH, Dan GOIA, Nicolae PAVEL, Richard E. MCLAUGHLIN and Lawrence TAMARKIN, 2004. Colloidal Gold: A Novel Nanoparticle Vector for Tumor Directed Drug Delivery. *Drug Delivery*. **11**(3), 169–183. ISSN 1071-7544. DOI: 10.1080/10717540490433895

40) PAINO, Maria Martinez I., Valéria S. MARANGONI, Rita de Cássia S. DE OLIVEIRA, Lusânia M. G. ANTUNES and Valtencir ZUCOLOTTO, 2012. Cyto and genotoxicity of gold nanoparticles in human hepatocellular carcinoma and peripheral blood mononuclear cells. *Toxicology Letters*. **215**(2), 119–125. ISSN 03784274. DOI: 10.1016/j.toxlet.2012.09.025

41) PITSILLIDES, Costas M., Edwin K. JOE, Xunbin WEI, R. Rox ANDERSON and Charles P. LIN, 2003. Selective Cell Targeting with Light-Absorbing Microparticles and Nanoparticles. *Biophysical Journal*. **84**(6), 4023–4032. ISSN 00063495. DOI: 10.1016/S0006-3495(03)75128-5

42) RASCHKE, Gunnar, Stefan KOWARIK, Thomas FRANZL, Carsten SONNICHSEN, Alfons NICHTL and Konrad KURZINGER, 2003. Biomolecular Recognition Based on Single Gold Nanoparticle Light Scattering. *Nano Lett.* **3**(7), 4.

43) ROJANATHANES, Rojrit, Amornpun SEREEMASPUN, Nuttaporn PIMPHA, Vanida BUASORN, Prapawadee EKAWONG and Viroj WIWANITKIT, 2008. Gold Nanoparticle as an Alternative Tool for a Urine Pregnancy Test. *Taiwanese Journal of Obstetrics and Gynecology*. **47**(3), 296–299. ISSN 10284559. DOI: 10.1016/S1028-4559(08)60127-8

44) ROMA-RODRIGUES, Catarina, Luís RAPOSO, Rita CABRAL, Fabiana PARADINHA, Pedro BAPTISTA and Alexandra FERNANDES, 2017. Tumor Microenvironment Modulation via Gold Nanoparticles Targeting Malicious

Exosomes: Implications for Cancer Diagnostics and Therapy. *International Journal of Molecular Sciences*. **18**(1), 162. ISSN 1422-0067. DOI: 10.3390/ijms18010162

45) SADAUSKAS, Evaldas, Gorm DANSCHER, Meredin STOLTENBERG, Ulla VOGEL, Agnete LARSEN and Hakan WALLIN, 2009. Protracted elimination of gold nanoparticles from mouse liver. *Nanomedicine: Nanotechnology, Biology and Medicine*. **5**(2), 162–169. ISSN 15499634. DOI: 10.1016/j.nano.2008.11.002

46) SADAUSKAS, Evaldas, Hakan WALLIN, Meredin STOLTENBERG, Ulla VOGEL, Peter DOERING, Agnete LARSEN and Gorm DANSCHER, 2007. Kupffer cells are central in the removal of nanoparticles from the organism. *Particle and Fibre Toxicology*. **4**(1), 10. ISSN 1743-8977. DOI: 10.1186/1743-8977-4-10

47) SMITH, Andrew M., Michael C. MANCINI and Shuming NIE, 2009. Second window for *in vivo* imaging: Bioimaging. *Nature Nanotechnology*. **4**(11), 710–711. ISSN 1748-3387. DOI: 10.1038/nnano.2009.326

48) SONAVANE, Ganeshchandra, Keishiro TOMODA and Kimiko MAKINO, 2008. Biodistribution of colloidal gold nanoparticles after intravenous administration: Effect of particle size. *Colloids and Surfaces B: Biointerfaces*. **66**(2), 274–280. ISSN 09277765. DOI: 10.1016/j.colsurfb.2008.07.004

49) SPERLING, Ralph A., Pilar R. GIL, Feng ZHANG, Marco ZANELLA and Wolfgang J. PARAK, 2008. Biological applications of gold nanoparticles. *Chemical Society Reviews*. **37**(9), 1896. ISSN 0306-0012. DOI: 10.1039/b712170a

50) STÖBER, Werner, Arthur FINK and Ernst BOHN, 1968. Controlled growth of monodisperse silica spheres in the micron size range. *Journal of Colloid and Interface Science*. **26**(1), 62–69. ISSN 00219797. DOI: 10.1016/0021-9797(68)90272-5

51) SU, Kai-Hung, Qi-Huo WEI, Xiang ZHANG, Jack. J. MOCK, David. R. SMITH and Sheldon SCHULTZ, 2003. Interparticle Coupling Effects on Plasmon Resonances of Nanogold Particles. *Nano Letters*. **3**(8), 1087–1090. ISSN 1530-6984. DOI: 10.1021/nl034197f

52) TEMPLETON, Allen C., Peter W. WUELFING and Royce W. MURRAY, 2000. Monolayer-Protected Cluster Molecules. *Accounts of Chemical Research*. **33**(1), 27–36. ISSN 0001-4842. DOI: 10.1021/ar9602664

53) TERENTYUK, Georgy S., Galina N. MASLYAKOVA, Leyla V. SULEYMANOVA, Boris N. KHLEBTSOV, Boris Ya. KOGAN, Garif G. AKCHURIN, Alexander V. SHANTROCHA, Irina L. MAKSIMOVA, Nicolai G. KHLEBTSOV and Valery V. TUCHIN, 2009. Circulation and distribution of gold nanoparticles and induced alterations of tissue morphology at intravenous particle delivery. *Journal of Biophotonics*. **2**(5), 292–302. ISSN 1864063X. DOI: 10.1002/jbio.200910005

54) VIGDERMAN, Leonid, Pramit MANNA and Eugene R. ZUBAREV, 2012. Quantitative Replacement of Cetyl Trimethylammonium Bromide by Cationic Thiol Ligands on the Surface of Gold Nanorods and Their Extremely Large Uptake by Cancer Cells. *Angewandte Chemie International Edition*. **51**(3), 636–641. ISSN 14337851. DOI: 10.1002/anie.201107304

55) ZANGANEH, Saeid, Ryan SPITLER, Mohsen ERFANZADEH, Alaaldin M. ALKILANY and Morteza MAHMOUDI, 2016. Protein corona: Opportunities and challenges. *The International Journal of Biochemistry & Cell Biology*. **75**, 143–147. ISSN 13572725. DOI: 10.1016/j.biocel.2016.01.005

56) ZARSKA, Monika, Filip NOVOTNY, Filip HAVEL, Michal SRAMEK, Andrea BABELOVA, Oldrich BENADA, Michal NOVOTNY, Hilal SARAN, Kamil KUCA, Kamil MUSILEK, Zuzana HVEZDOVA, Rastislav DZIJAK, Marketa VANCUROVA, Katerina KREJCIKOVA, Blanka GABAJOVA, Hana HANZLIKOVA, Lenka KYJACOVA, Jiri BARTEK, Jan PROSKA and Zdenek HODNY, 2016. Two-Step Mechanism of Cellular Uptake of Cationic Gold Nanoparticles Modified by (16-Mercaptohexadecyl)trimethylammonium Bromide. *Bioconjugate Chemistry*. **27**(10), 2558–2574. ISSN 1043-1802. DOI: 10.1021/acs.bioconjchem.6b00491

57) ZARSKA, Monika, Michal SRAMEK, Filip NOVOTNY, Filip HAVEL, Andrea BABELOVA, Blanka MRAZKOVA, Oldrich BENADA, Milan REINIS, Ivan STEPANEK, Kamil MUSILEK, Jiri BARTEK, Monika URSINYOVA, Ondrej

NOVAK, Rastislav DZIJAK, Kamil KUCA, Jan PROSKA and Zdenek HODNY, 2018. Biological safety and tissue distribution of (16-mercaptohexadecyl) trimethylammonium bromide-modified cationic gold nanorods. *Biomaterials*. **154**, 275–290. ISSN 01429612. DOI: 10.1016/j.biomaterials.2017.10.044

58) ZHANG, Guodong, Zhi YANG, Wei LU, Rui ZHANG, Qian HUANG, Mei TIAN, Li LI, Dong LIANG and Chun LI, 2009. Influence of anchoring ligands and particle size on the colloidal stability and *in vivo* biodistribution of polyethylene glycol-coated gold nanoparticles in tumor-xenografted mice. *Biomaterials*. **30**(10), 1928–1936. ISSN 01429612. DOI: 10.1016/j.biomaterials.2008.12.038

8. List of Figures and Tables

membrane-specific staining was done with WGA, nuclei by DAPI + detection of [MTAB]GNRs.

Fig. 17 – Gold nanoparticles of various size and shape with potential applications in biomedicine (Dreaden *et al.* 2012).

<u>**TABLES:**</u>

Tab. 1 – The list of used chemicals.

Tab. 2 – The list of used antibodies.

Tab. 3 – An overview of the consecutive time selected studies in rodents through exposure of intravenous injection.

Tab. 4 – Classification of CD markers for immunophenotyping.
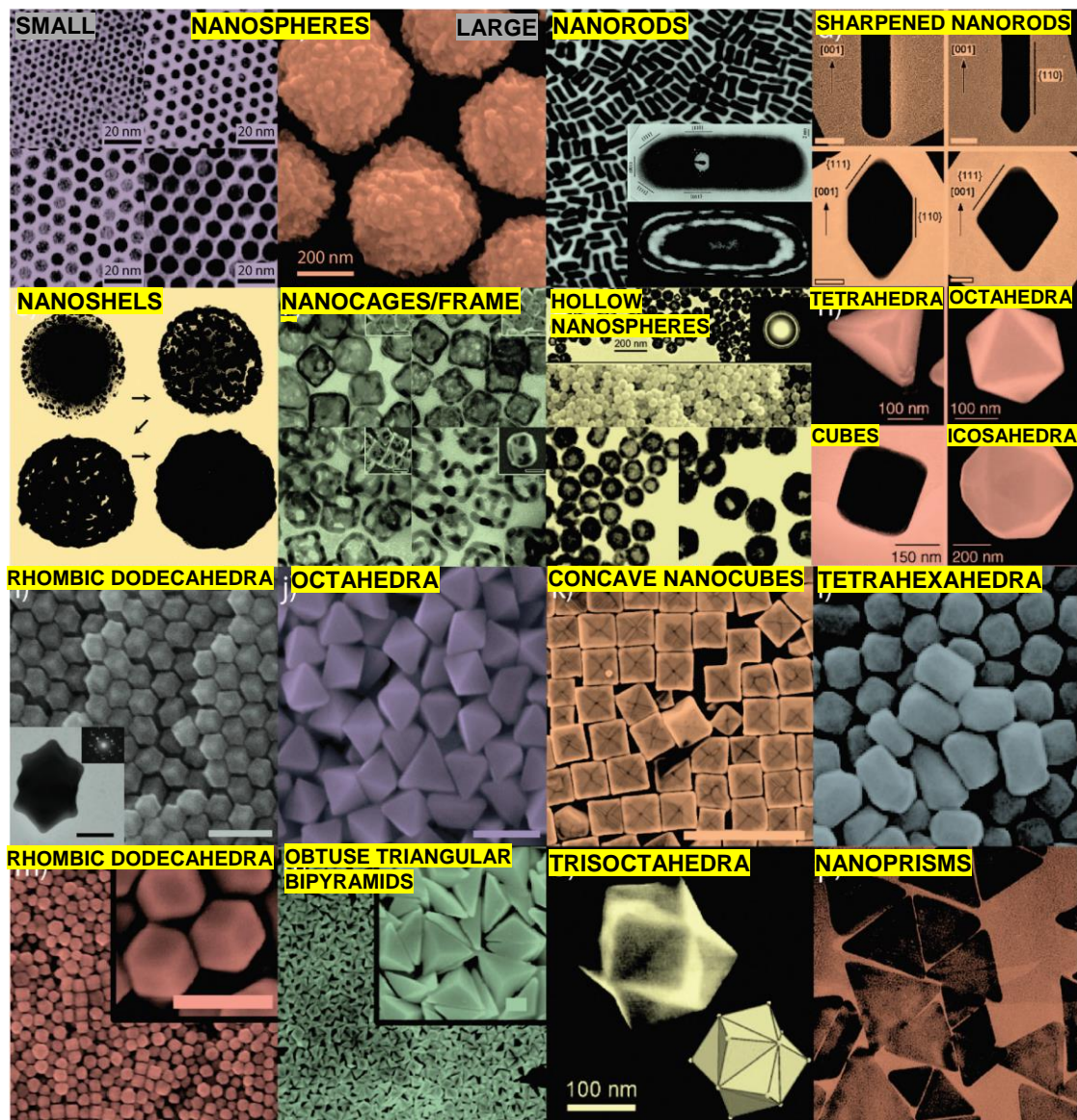
9. Attachments

Fig. 17 – Gold nanoparticles of various size and shape with potential applications in biomedicine (Dreaden *et al.* 2012).

Tab. 3 – An overview of the consecutive time selected studies in rodents through exposure of intravenous injection.

Reference	Model	GNPs	Duration	Dose [mg/kg]	Organs examined
Hainfeld *et al.* 2004	Mice	1.9 nm	5 min	1350–2700	5
Paciotti *et al.* 2004	Mice	33 nm (PEG–SH)	6 h	0.3–0.6	5
Bergen *et al.* 2006	Mice	50, 80, 100, 150 nm (unmodified; PEG$_{5000}$–SH; gal–PEG–O–pyridyl disulphide)	2 h	0.5–0.6	3
Hainfeld *et al.* 2006	Mice	1.9 nm	24 h	700, 70, 7	5
Niidome *et al.* 2006	Mice	Nanorods (65x11 nm)	0.5, 3, 6, 12, 24, 72 hours	0.98–1.52	5
Balogh *et al.* 2007	Mice	5, 22 nm–positive; 5, 11 nm–negative; 5 nm–neutral	5 min; 1 h; 1, 4, 7 days	16	10 (+ faeces; urine)
Sadauskas *et al.* 2007	Mice	2 and 40 nm	1, 4, 24 hours	0.6–3.2	8
De Jong *et al.* 2008	Rat	10, 50, 100, 250 nm	24 h	70–120 µg/mL	13
Huang *et al.* 2008	Mice	Au–Au$_2$S	7 days	10	10
Sonavane *et al.* 2008	Mice	15, 50, 100, 200 nm	24 h	1000	9
Cho *et al.* 2009	Mice	13 nm (PEG–SH)	5, 30 min; 4, 24 h; 7 days	0.17–4.26	7
Sadauskas *et al.* 2009	Mice	40 nm	1 day; 1, 3, 6 months	1.4–1.6	Liver
Terentyuk *et al.* 2009	Rat	15, 50, 160 nm (PEG–SH)	24 h	57 µg/mL	6
Zhang *et al.* 2009	Mice	20, 40, 80 nm (PEG–SH; ^{111}In)	48 h	0.1–4.4	11
Balasubramanian *et al.* 2010	Rat	20 nm	1 day; 1 week; 1, 2 months	0,01	28 (+ faeces; urine)
Zarska *et al.* 2018	Mice	Nanorods (54x26 nm; MTAB)	24 h; 10 days	0.37; 1.8	5 (+ blood)

(Redesigned from Balasubramanian *et al.* 2010).

Tab. 4 – Classification of CD markers for immunophenotyping.

Type of cells	CD marker
WBCs	CD45+
Neutrophils	CD15+, CD16+, CD68+,
Eosinophils	CD15+, CD16-
Basophils	CD123+, CD33+, CD22+
B-lymphocytes	CD19+, CD20+
T- lymphocytes	CD3+
➢ T-helper	CD3+, CD4+
➢ T-cytotoxic	CD3+, CD8+
Monocytes	CD14+

(Redesigned from Hořejší and Bartůňková 2005).

10. Abbreviations

AAS – atomic absorption spectroscopy

AOBS – acoustic-optical beam splitter

Au^0 – metallic gold

BSA – bovine serum albumin

CD – cluster of designation

^{CITRATE}GNPs – gold nanoparticles modified with citrate

CT – computed tomography

CTAB – cetyltrimethylammonium bromide

^{CTAB}GNRs – gold nanorods modified by cetyltrimethylammonium bromide

DAPI – diamidino–phenylindole

DLS – dynamic light scattering

DMEM – Dulbecco's Modified Eagle Medium

DPX – a mixture of distyrene, a plasticizer and xylene

EDTA – ethylenediaminetetraacetic acid

FE–SEM – field emission scanning–electron microscopy

FITC – fluorescein isothiocyanate

GNPs – gold nanoparticles

GNRs – gold nanorods

HBSS – Hank's balanced salt solution

hCG – human gonadotropin

^{1}H NMR – proton nuclear magnetic resonance

HSA – human serum albumin

ICP-MS – inductively coupled plasma-mass spectrometry

LSPR – localized surface plasmon resonance

MTAB – (16–mercaptohexadecyl)trimethylammonium bromide

^{MTAB}GNRs – GNRs modified by (16–mercaptohexadecyl)trimethylammonium bromide

NIR – near infrared

PBMCs – peripheral blood mononuclear cells

PBS – phosphate buffered saline

PEG – poly(ethylene glycol)

PEG-SH – poly(ethylene glycol) methyl ether thiol

PEO – poly(ethylene oxide)

RBCs – red blood cells

RP – red pulp

SEM – scanning electron microscopy

shRNA – short hairpin RNA

siRNA – small interference RNA

TEM – transmission electron microscopy

THPC – tetrakis(hydroxymethyl) phosphonium chloride

TNF – tumour necrosis factor

UV-VIS – ultraviolet-visible spectroscopy

WBCs – white blood cells

WGA – wheat germ agglutinin

WP – white pulp